Transient pressure waves in the vadose zone and the rapid water table response

George W. Waswa†, Alistair D. Clulow, Carl Freese, Peter A.L. Le Roux, and Simon A. Lorentz

George W. Waswa, School of Engineering; Alistair D. Clulow, Carl Freese, and Simon A. Lorentz, School of Agricultural, Earth and Environmental Sciences, University of KwaZulu-Natal, Private Bag X01, Scottsville 3201, South Africa; Peter A.L. Le Roux, Department of Soil, Crop and Climate Sciences, University of the Free State, P.O. Box 339 Bloemfontein 9300, South Africa. Received _____ *Corresponding author (208529656@stu.ukzn.ac.za).

ABSTRACT

The behaviour of a water table is important in understanding groundwater dynamics. In this paper, results are presented of a disproportionate response of a water table in two distinct transient pressure wave mechanisms that occurred during the rainfall events of the 2000/2001 summer season and in two different hillslope zones in the Weatherley research catchment of South Africa. The first type of pressure wave mechanism was a groundwater ridging pressure wave, which frequently occurred at the low-lying wetland zone and when the capillary fringe was very close to the ground surface. Results from this zone indicated that groundwater ridging water table responses were caused by rainfall events that had a threshold total rainfall of 10 mm and the magnitude of the responses had a linear relationship with the peak rainfall intensities. It was also found that the release of tension forces in the capillary fringe, due to the downward pressure wave, was 2.5 to 22.5 times faster than the subsequent rise of the water table (the upward pressure wave). This later finding, according to the law of conservation of energy, indicated an on-set of a lateral flow of water, below the rising water table. The second pressure wave mechanism, which exhibited the characteristics of the Lisse Effect (pneumatically pressurized water table response), occurred at an elevated zone of the

† Corresponding author address: University of KwaZulu-Natal, School of Engineering, Pietermaritzburg Campus, Rabie Saunders Building, Room 220B, P.O. Private Bag, X01, 3209, Scottsville, South Africa. Tel: +27-33-2606055, Fax: +27-33-260 5818. E-mail : 208529656@stu.ukzn.ac.za

catchment, where bedrock is overlain by a shallow soil profile and a perched groundwater. This second pressure wave mechanism was particularly evident during a certain rainfall event that occurred in the early part of the season. During this rainfall event, a peak rainfall intensity of 228 mm/h generated a pressure wave from the ground surface towards the water table, where it rapidly and disproportionately elevated the hydraulic head in groundwater by 106 cm-H_2O, at the toe of the slope and without the recharge of the groundwater by the infiltration profile. The elevated hydraulic head at the toe of the slope rapidly overturned the hydraulic gradients, from 0.0100, in the downslope direction, to 0.0105, in the upslope direction, in just 24 minutes. The overturned hydraulic gradients reversed the flow of water from a downslope direction to an upslope direction. The overturning wave, which originated with an elevated pressure potential of 106 cm-H_20, at the downslope observation nest, travelled with an average velocity of 2 m/h and arrived at an adjacent observation nest, 46 m up the slope, with an attenuated pressure potential of 31 cm-H_2O. A laboratory experiment was performed to verify this second transient pressure wave mechanism and to investigate the involved processes. Results from the laboratory experiment verified that the second pressure wave was the Lisse Effect and that, as in the groundwater ridging, the capillary fringe plays a significant role in the rapid response of the water table. In conclusion, both the Lisse Effect and groundwater ridging may result in disproportionate groundwater fluxes, which is successively caused by the conversion of the capillary fringe and a disproportionately rapid water table rise. **Key words:** *groundwater fluxes, groundwater ridging, hydraulic gradient, the capillary fringe, the Lisse Effect*.

1. Introduction

Previous studies (e.g. Pinder and Jones, 1969, Sklash and Farvolden, 1979 and Wenninger *et al.*, 2004) have shown that during a rainfall event, pre-event water, which is predominantly

groundwater, may appear in significant amounts in the stream stormflow hydrograph. Therefore, a comprehensive understanding of the dynamics of groundwater fluxes is important. However, in order to understand groundwater dynamics and the appearance of pre-event water in the stormflow hydrograph, it is necessary to understand the behavior of the groundwater table response during a rainfall event.

Mechanisms that have been reported in literature of a rapid water table response during a rainfall event, include: (1) the cessation of the water uptake by plants, which might occur, as a result of the reduction in evapotranspiration caused by cooler temperatures, wet leaf and long diminished sunlight hours (White, 1932 cited in Heliotis and DeWitt, 1987); (2) macropores, which enhance the rapid delivery of rain water to the water table (McDonnell, 1990); (3) groundwater ridging (Gillham, 1984); (4) the Lisse Effect (Heliotis and DeWitt, 1987 and Weeks, 2002); and (5) the near-zero pressure-head-range pressure wave (Torres *et al.*, 1998). The latter three mechanisms are caused mainly by pressure waves, generated from the ground surface and transmitted through the vadose zone to the water table. Consequently, the water table responds rapidly to the changes in pressure and not to the recharge from the infiltration profile. Furthermore, these three mechanisms have also been proposed to account for the rapid mobilization of pre-event water from hillslopes (e.g. Gillham, 1984, Lorentz *et al.*, 2004 and Torres *et al.*, 1998).

The groundwater ridging has been commonly observed in environments, where the water table is shallow and the capillary fringe, or the zone of tension saturation, extends to, or intersects with, the ground surface. In such environments, it has been found (e.g. Abdul and Gillham, 1989 and Gillham, 1984) that the addition of a small amount of water results in a disproportionate rise of the water table, compared with the expected rise from the specific

yield concept. Gillham (1984), for instance, reported a field experiment, in which an addition of 0.3 cm of water in an area with a shallow water table resulted in a 30 cm rise of the water table in 0.25 minutes. Later, Abdul and Gillham (1989) carried out field experiments on a plot measuring 18 m wide by 90 m long and traversed by a stream channel. These researchers applied a simulated rainfall over the plot, using a sprinkler irrigation system and observed a disproportionate rise of the water table, which was attributed to the initial proximity of the capillary fringe to the ground surface. Apart from field experiments, laboratory experiments (Abdul and Gillham, 1984; Heliotis and DeWitt, 1987 and Khaled *et al.*, 2007) and theoretical and numerical modeling approaches (Jayatilaka and Gillham, 1996; Jayatilaka *et al.*, 1996 and Khaled *et al.*, 2011) have been used to evaluate groundwater ridging. It seems that most of the studies on groundwater ridging have been limited mainly to partially-controlled field experiments, fully-controlled laboratory experiments and theoretical/numerical simulations. Lack of observations of groundwater ridging in the field conditions has generated skepticism among researchers regarding its practicability under natural rainfall (Buttle and Sami, 1992 and McDonnell and Buttle, 1998).

The Lisse Effect may occur in environments, where the water table is deep enough to allow an unsaturated zone, with a sufficient and continuous volume of pore air, above the capillary fringe. During an intense rainfall, or a flooding event, on the ground surface, an infiltration profile is generated, which may cap the ground surface and engulf air ahead of the wetting front. If the lateral escape routes of air are limited, due to the tortuosity of the pathways; and the vertical counterflow of air is imbedded by an infiltration profile; further downward movement of the wetting front compresses and increases the pore air pressure ahead of the wetting front. The increased pressure in air is immediately transferred; in an action process, to the water table below and; in a reaction process, to the wetting front above. The reaction

effect of compressed pore air on infiltration has been widely studied (Adrian and Franzini, 1966; McWhorter, 1971; Touma *et al.*, 1984; Wang *et al.*, 1998). The action of compressed pore air on the water table contributes to the pressure potential term in the groundwater, which is reflected in the rapid rise of a water level in a well, screened below the water table (Weeks, 2002). The action of compressed pore air influences the flow of water by way of total potential gradient (Bond and Collis-George, 1981). It has been noted that the Lisse Effect occurs in areas with rainfall of high magnitude and intensity, which may result in disproportionate rises in water levels that are 50-250 % higher than predicted from the specific yield (Heliotis and DeWitt, 1987; Weeks, 2002). Nevertheless, the physical processes, by which the Lisse Effect rapid water table response occurs, are not yet clear.

The near-zero pressure head range pressure wave was first observed in the field experiments and described in detail by Torres *et al.*, (1998), and latter observed in column experiments by (Rasmussen *et al.*, 2000). By the application of steady irrigation rates on the ground surface, Torres *et al.* (1998) maintained dynamic equilibrium conditions between groundwater discharge, saturated zone and the unsaturated zone, which was at near-zero pressure head. Under these conditions, an application of a spiked intensity rainfall, caused a rapid pressure wave through the unsaturated zone, followed by a disproportionately rapid response in the saturated zone and groundwater discharge. Torres *et al.* (1998) explained that the rapid pressure wave may have elevated the hydraulic head gradient that caused a rapid effusion of stored pre-event water from the unsaturated zone. The effused pre-event water caused the rapid rise in the saturated zone and thus, increased groundwater discharge.

This paper distinguishes between a deep water table and a shallower water table by the position of the capillary fringe, with respect to the ground surface. A deep water table occurs,

where the capillary fringe is far below the ground surface, to allow a sufficient depth of unsaturated zone, with a continuous pore air, in that the Lisse Effect may occur during an intense rainfall. A shallow water table occurs, where the capillary fringe is close to, or intersects with, the ground surface. Furthermore, in this paper, a capillary fringe is defined as a zone of tension saturation. That is, the zone immediately above a water table, in which all the soil pores are filled with water, which is under tension pressure.

The objectives of this paper are: (1) to describe and analyze the rapid response of a water table in a groundwater ridging transient pressure wave mechanism that frequently occurred at a wetland zone of the study catchment; (2) to describe and analyze the rapid response of a water table to a transient pressure wave mechanism (which exhibited the characteristics of the Lisse Effect) that occurred during a certain rainfall event and in a raised zone of the study catchment; and (3) using a laboratory experiment, to verify the nature of the second transient pressure wave mechanism (in 2 above) and evaluate the involved physical processes.

2. Methodology

2.1 Field study site

2.1.1 Field set up

The field data were from observations made in two different hillslope zones of the Weatherley research catchment, which is located in the uMzimvubu Water Management Area (WMA) in the north-eastern Cape Province of South Africa (Fig. 1). The catchment lies at a latitude of 31^{o} 06’ 00’’ S, a longitude of 28^{o} 20’ 10’’ E and at an altitude of approximately 1300 m. The average annual rainfall in the catchment is about 740 mm, of which 82 % is received between October and March (summer period) (Lorentz *et al.*, 2001). The catchment, which covers an

150 area of 1.5 km^2 and drains in a northerly direction, contains a wetland that lies along the entire
151 reach of the stream.
152
153 About 200 m from the stream, in an easterly direction, there is a bedrock outcrop (between
154 observation nests L4 and L5, in Fig. 1), which runs almost parallel to the stream. The bedrock
155 outcrop is about 12 m in altitude above the stream bed. This bedrock forms a shelf, over
156 which lies a varying depth of soil. This area, henceforth referred to as 'a hillslope zone,' is
157 one of the two zones, from where a water table response to a transient pressure wave was
158 analyzed. The data used in the analysis were from the observation nests L2, L3 and L4 (also
159 shown in Fig. 2). At this zone, the average depth of the soil profile to bedrock varies from 2.5
160 m at the peak of the hillslope (near L1), to about 3.5 m in the middle of the slope (at L3) and
161 thins out to zero at the bedrock outcrop (a few metres in the downslope of L4). The absolute
162 length of the bedrock, and thus of the hillslope zone, is about 250 m (Fig. 2). The second zone
163 used in the analysis of rapid water table response is the wetland zone. This zone was selected
164 because, according to the literature (e.g. Gillham, 1984; Heliotis and DeWitt, 1987),
165 groundwater ridging rapid water table response is most likely to occur at the wetland or
166 swampy areas. At the wetland zone, for this part of the study, data from observation nests U3,
167 U4 and the stream discharge over the upper weir, were used.
168
169 At the present time, the land-cover over the catchment consists of patches of trees, which
170 were planted in 2002, and patches of highland sourveld grassland. Typical grass species
171 include *Themeda triandra* and *Tristachya leuctthrix*. Succulent species of the group *Aloe* and
172 *Crassula* are common at shallow slopes. Generally, these grass species have shallow root
173 systems. At the hillslope zone, the forested area covers observation nests L2 and L3, while
174 ground cover at observation nest L1 and L4 is mainly grass. Recent observations indicate that

175 the establishment of trees in this zone of the catchment has resulted in the depletion and
176 complete absence of groundwater in some areas, especially at L3. The entire wetland zone is
177 covered by shallow rooted grass.
178
179 **2.1.2 Soil physical properties**
180 At the hillslope zone, the soils are generally sandy loam in the upper horizons and sandy clay
181 in the lower horizons. The dominant infiltration mechanism in the areas that are covered by
182 grass is through the soil matrix. There might be small macropores, due to small holes left by
183 rotten vegetation roots, but they hardly extend below 10 cm below the ground surface.
184 Therefore, infiltration by preferential flow is generally insignificant. At the upper sub-
185 catchment wetland zone, sandy loam soil and loamy clay soil appear at U1-U3 nest-axis and
186 U4-U8 nest-axis, respectively. The specific physical soil properties i.e. hydraulic
187 conductivities, bulk densities and porosity at each of the selected observational nests, are
188 shown in Table 1. The hydraulic properties, specifically water retention characteristics and
189 hydraulic conductivities, were determined both in the field and in the laboratory (Klute and
190 Dirksen, 1986 and Bruce and Luxmore, 1986). Field measurements at each of the indicated
191 depths (Table 1) of the soil profile were carried out by tension disc and double ring
192 infiltrometers. Undisturbed cores of soils were sampled from the indicated depths for
193 laboratory tests, which included water retention characteristics, saturated hydraulic
194 conductivities, bulk densities and particle size distribution. This set of data was obtained from
195 Lorentz *et al.* (2001). During the present investigation, tests of particle size distribution of the
196 soil samples, from observations nests U3 and L4, were determined in the laboratory (Table 1).
197

198 **2.1.3 Instrumentation**

199 The instrumentation and observations programme in the Weatherley research catchment
200 started in 1995 to provide necessary data for the evaluation of the impact of forestation on the
201 hydrological processes in the catchment (Wenninger *et al.*, 2008). The catchment was
202 monitored in its pristine state up to 2002, when a section of the catchment's area was
203 afforested (*Pinus Patula*, *Pinus Elliotti* and *Ecalyptuc Nitens*). Each observation nest at the
204 hillslope zone consisted of a groundwater observation hole, installed to bedrock, for
205 monitoring groundwater levels, as well as ceramic-cup tensiometers installed at different
206 depths in the soil profile (Fig. 2), for the measurement of the soil pore water pressure. The
207 observation nests U3 and U4 did only have tensiometers. Therefore, the water table responses
208 at these nests were analyzed based on the soil pore water pressure, in which positive and
209 negative pressure potentials imply a water table above and below the point of measurement,
210 respectively. At U3, the ceramic cups of the shallower and deeper tensiometers were installed
211 at 20 cm and 100 cm below the ground surface, respectively. At U4, the ceramic cup of the
212 shallower tensiometer was at 30 cm and that of the deeper tensiometer was at 110 cm, below
213 the ground surface.
214
215 Rainfall data were recorded via a tipping-bucket rain gauge, with an accumulation of 0.2 mm
216 of rainfall per tip. The rain gauge logger recorded the data at one minute intervals. A detailed
217 description of the catchment is found in Lorentz *et al.* (2001), Lorentz *et al.* (2004) and
218 Wenninger *et al.* (2008).
219
220 Between November 1999 and April 2005, the data of tensiometric pore water pressure and
221 water levels were monitored, recorded and stored automatically on Onset HOBO loggers.
222 Both the data of pore water pressure, as well as of the water level, were transmitted and

temporarily stored on Onset HOBO loggers via I bar Motorola MPX5100DP differential pressure transducers. This set of data was recorded with a time resolution of 12 minutes. The field data used in the present study was of the summer season of 2000/2001, when the observation programme was fully automated and prior to the establishment of trees. The summer season of 2000/2001 was selected because it had the best data in terms of continuity, compared to other observation periods.

2.1.4 Rainfall events

The responses of the water table were analyzed, based on rainfall events, which were based on the period above a minimum threshold of rain. Six hours, with less than 1.2 mm of rainfall, was chosen as the boundary between sequential rainfall events. For each rainfall event, hourly rainfall depths, as well as one-minute rainfall intensity, were computed.

2.2 Laboratory Experiment

2.2.1 Laboratory apparatus

The physical laboratory model consisted of a column of soil in a vertical PVC pipe with an internal diameter of 30 cm and a height of 300 cm. The soil was graded silica quartz (SiO_2), which was uniform in shape and the individual grains were stable and clean, free of organic matter. The particle size distribution, the saturated hydraulic conductivity and the water retention characteristics of sand were determined in the laboratory following the methods and procedures of Gee and Bauder (1986), Klute (1986) and Klute and Dirksen (1986), respectively. The values of the physical properties of the soil used are shown in Table 1.

Seven data takeoff ports were installed along the pipe, at 60, 90, 120, 130, 140, 150 and 160 cm below the soil surface, which was at 40 cm below the top of the PVC pipe. Each data

248 takeoff port consisted of three probes: a 0.5 bar miniature tensiometer for the measurement of
249 soil pore water pressure, a Time Domain Reflectometry (TDR) for the measurement of
250 volumetric water content and a pore air pressure probe for the measurement of pore air
251 pressure. A drainage/discharge tube and a piezometer were attached to the column at a depth
252 of 170 cm below the soil surface, for groundwater discharge and monitoring of the water
253 table, respectively.
254
255 The TDR probes used were made of three parallel stainless steel rods with, an exposed length
256 of 100 mm, a diameter of 5 mm, impeded in a PVC block and at a separation distance of 17
257 mm. The soil water content data, measured by TDR, were recorded and temporarily stored on
258 a CR1000 Campbell Scientific data logger via a SDMX50 Multiplexer and Campbell
259 Scientific TDR100 wave generator. Miniature tensiometers consisted of a 15 mm-long
260 ceramic-cup, with an outer diameter of 5 mm. The open end of the ceramic cup was joined to
261 one end of a PVC tube with the same outer diameter. The other end of the PVC tube was
262 connected to a differential pressure transducer. The data of pore-water pressure and pore-air
263 pressure were recorded and temporarily stored on a CR1000 Campbell Scientific data logger
264 via differential pressure transducers of 1 bar Motorola MPX5100DP and 0.1 bar Motorola
265 MPX5010DP, respectively.
266
267 The pore-air pressure probe was developed for the measurement of compressed pore air. The
268 probe was made of a PVC cylindrical solid rod, 14 cm long and 2 cm in diameter and with a
269 hydrophobic membrane (see Fig. 3). Holes, of 5 mm diameter, were drilled across the PVC
270 cylindrical solid. These transverse holes, which were drilled over a 5 cm length-portion of the
271 cylindrical solid, were orthogonally traversed by a 2 mm diameter hole made in the
272 longitudinal centre of the rod. The 2 mm diameter longitudinal hole only penetrated the

cylindrical solid at the back end. The section of the probe, over which the transverse holes were made, was recessed and wrapped in a hydrophobic membrane, which allowed only the passage and flow of air. The hydrophobic membrane only allowed the passage of water at very high pressures, >5 cm-H_2O. A short, 5 mm diameter PVC tube, linked the probe from its back end to the differential pressure transducer. For ease of installation, the front end of the probe was made pointed.

In the remaining part of this paper, for brevity and ease of reference, a specific data-takeoff port will be referred to as 'Port', followed by its depth, below the soil surface. For example, 'Port 60' refers to the data take-off port, which is also located at 60 cm below the soil surface. All the pressures reported in this paper are in height of water, specifically cm-H_2O.

2.2.2 Experimental procedure

The PVC cylindrical pipe was packed with dry silica sand, in layers of ~55 cm high. After each layer, the wall of the pipe was tapped with the same number of blows, in order to achieve uniform maximum density and packing. The TDRs and the pore-air pressure probes were inserted in the wall of the PVC pipe before being packed with sand. The ceramic-cup miniature tensiometers, due to their fragility, were inserted after packing the column. All the probes were inserted into the column of soil and the entire wall of the pipe was sealed to an air-tight state.

Water was introduced in the packed column of soil from the bottom to minimize the entrapment of pore air, which has been found to contribute to disproportionate water table responses (Peck, 1960; Weeks, 1979). By adjusting the level of the nozzle of the discharge tube, the initial water table was set at Port 160, as shown in Fig. 4. The capillary fringe, of

298 which the height was taken as equivalent to the air-entry pressure value, or the bubbling
299 pressure, of the soil (Brooks and Corey, 1964, 1966), extended to about 20 cm above the
300 water table. The bubbling pressure of the soil is the pressure at which a continuous non-
301 wetting phase exists in a porous media. The initial conditions of the soil column were, as
302 shown in Fig. 4.
303
304 With the described set up, the experiment was initiated by ponding the soil surface with 15
305 cm of water. Groundwater fluxes, tensiometric pore water pressure, volumetric water content
306 and pore air pressure were monitored and recorded at a time-resolution of 20 seconds, starting
307 from the moment the soil surface was ponded.
308
309 **3. Results**
310 **3.1 Rainfall Events**
311 The total of 96 rainfall events occurred during the summer season of 2000/2001 in the
312 Weatherley research catchment. The general characteristics of the rainfall events are
313 summarized in Table 2. Only the rainfall events that caused rapid water table response, at the
314 selected observation nests at the wetland zone or/and at the hillslope zone are included. The
315 events are ordered according to their dates of occurrence. The total rainfall amount recorded
316 during this period was 947 mm, which was significantly above the mean annual precipitation
317 amount of 740 mm in this catchment (Lorentz *et al.*, 2004; Wenninger *et al.*, 2008). 70% of
318 the rainfall events were less than 10 mm. Event 19 had the highest rainfall, namely 67.8 mm,
319 as well as the highest peak 1-minute intensity, namely 228 mm/h.
320
321

3.2 Field observations of rapid water table responses to transient pressure waves

3.2.1 Rapid water table response to groundwater ridging transient pressure wave at a wetland zone

Responses of the soil pore water pressure at the observation nests U3 and U4, at the wetland zone, are shown in Fig. 5. The water table at U4 seems to have remained at the ground level from December 2000 and for the rest part of the season. This is attributed to the type of soil at U4, the heavy clay soil that did not easily drain, after saturation. The type of soil at U4 did not easily allow the passage of pressure due to the rainfall on the ground surface down the soil profile.

On the other hand, at U3, three main temporal phases are noted in the responses of the pore water pressure to the rainfall events. Phase 1 occurred during the months of September and October, in which the water table (capillary fringe) was still deep and the upper tensiometer recorded extremely dry conditions. The tensiometric pore water responses, to the rainfall events in Phase 1, are generally characterized by very large changes in pressure potential. In Phase 3, the water table was nearly always above the shallower tensiometer. Phase 2 begins from mid-November to mid-March and is characterized by the oscillation of the water table (zero pressure head) around the shallower tensiometer. It is worth noting that the two tensiometers exhibited a more uniform pattern during Phase 2 than in the other two phases. From the position of the shallower tensiometer below the ground surface, resonance of the water table around this shallower tensiometer, the water retention characteristics of the soil at this nest (h_a = 45 cm, Table 1) and the rapid and simultaneous responses of the two tensiometers, groundwater ridging transient pressure wave water table response may have occurred frequently during Phase 2. A close similarity can also be seen in the responses to the

rainfall events, of the tensiometers at U3 (Phase 2) and the stream discharge over the upper weir.

Factors that control the groundwater ridging water table response

An analysis was carried out to assess the effect of peak rainfall intensity and total rainfall depth on the pore water pressure responses, indicated by the shallower tensiometer at the observation nest U3. It was found that groundwater ridging only occurred in the rainfall events that had a minimum total rainfall depth of 10 mm (Fig. 6).

A separate analysis of the position of the water table, via the pressure potential values of the deeper tensiometer, indicated that in addition to the threshold rainfall amount, groundwater ridging pressure wave occurred only, when the water table was between 43.4 and 18.9 cm below the ground surface (Table 3, Col. 8). This requirement of the initial position of the water table explains the presence of the two outlier rainfall events (in Fig. 6), which yielded more than 10 mm of rainfall, but did not cause groundwater ridging water table response. In these two events, the initial water table was below the deeper tensiometer (>100 cm below the ground surface). This implies that the capillary fringe was too deep, for groundwater ridging to occur.

Similarly, the initial water table requirement indicates the significant role played by the soil water content, which can be inferred from; the time interval the end-time of one rainfall event and the start-time of the next rainfall event, as well as from the pre-event values of the pressure potentials. It was observed that all the events that caused groundwater ridging had a minimum separation time of 3.72 days between events (Table 3, Col. 9). This minimum separation time was required for drainage and recovery of the capillary fringe, before the

371 subsequent groundwater ridging pressure wave could occur. The role of the initial soil water
372 content in groundwater ridging was also inferred from initial values of pressure potential
373 recorded by the shallower tensiometer. For the events that caused groundwater ridging, the
374 shallower tensiometer recorded pre-event pressure potential values of between -1.30 and -
375 27.20 cm-H_2O. In events, where the total rainfall depth was greater than 10 mm and the
376 shallower tensiometer recorded higher values of pressure potential, a translatory or a piston
377 flow type of pressure wave might have occurred (Fig. 6).
378
379 A general linear relationship was identified between the intensity of rainfall and the total
380 reaction of the shallower tensiometer (Fig. 7). This linear relationship implies that the higher
381 the rainfall intensity, the larger the response of the water table. The influence of rainfall depth
382 and intensity on groundwater ridging water table response, for two representative rainfall
383 events, is schematically shown in Fig. 8.
384
385 Fig. 8 (a) is the response of the tensometers to the rainfall Event No. 43, which had a total
386 rainfall depth of 20 mm and a peak intensity of 18 mm/h. Fig. 8 (b) is the response of the
387 tensometers to the rainfall Event No. 70, which had a total rainfall depth of 47.2 mm and a 1-
388 minute peak intensity of 102 mm/h. The pre-event pressure potential values of the shallower
389 tensiometer, in the two events, were -27.2 cm-H_2O and -23.6 cm-H_2O, respectively. However,
390 the rate of, and the total response of, the shallower tensiometer, were proportional to the total
391 rainfall depth and peak intensity (Fig. 8). Furthermore, in Fig. 8, a very important feature is
392 noted: the refraction (the rate of change in response) in the pressure curves of the shallower
393 tensiometer, as soon as they cross the zero pressure line. Bearing in mind that the shallower
394 tensiometer was within the capillary fringe, which extended close to the ground surface, the
395 section of the pressure curve before the zero pressure line represents the release of the tension

396 forces (caused by the downward pressure wave) in water within the capillary fringe, while the
397 section after the zero pressure line represents the rising water table (upward pressure wave).
398 An analysis of the pressure curves of the shallower tensiometer, for all the events that caused
399 the groundwater ridging water table response, indicated that its rate of reaction to the
400 downward pressure wave was 2.5 to 22.5 times its rate of reaction to the upward pressure
401 wave.
402
403 **3.2.2 Rapid water table response to a transient pressure wave at a hillslope zone**
404 The results of soil pore water pressure and water level responses to the rainfall events of the
405 summer season of 2000/2001 at the observational nests L2, L3 and L4 at the hillslope zone,
406 are shown in Fig. 9. From the responses of the water level and tensiometric pore water
407 pressure at L2, in Fig. 9 (e) and Fig. 9 (f), respectively, it can be seen that the lower horizons
408 of the soil profile at this nest remained at constant saturation throughout the season. This
409 observation is made from the nearly constant pore water pressure recorded by the deepest
410 tensiometer and the nearly constant water level in the observation hole. This implies no
411 recharge of the groundwater. However, the two shallower tensiometers responded, more
412 often, in a uniform pattern consistent with the rainfall events.
413
414 Down the slope, at L3, the water level responses displayed fluctuations in the water table (Fig.
415 9 c), which indicated recharge and drainage of the groundwater. However, there seems to be
416 no common pattern in the responses of the water level and the responses of the tensiometric
417 pore water pressure at L3 (Fig. 9 d). This implies that the water table fluctuations at L3 was
418 not caused by the recharge from above. This can also be noted in the disconnection between
419 the responses of the two shallower tensiometers (tens @ 20 cm and tens @ 50 cm) and the
420 deepest tensiometer (tens @ 80 cm) at L3 (Fig. 9 d). While the two shallower tensiometers

421 rapidly and uniformly responded to the rainfall events, the magnitude of these responses
422 diminished with depth; the deepest tensiometer responding only to fewer rainfall events. This
423 implies that the infiltration front, to which the two shallower tensiometers responded, did not,
424 in many rainfall events, reach the deepest tensiometer. These observations concur with those
425 of Lorentz *et al.* (2004), who found that the percolation to the water table, of the infiltration
426 front at L3 is generally slow. It is also worth noting that, while the two shallower tensiometers
427 reacted almost at the same rate, their recovery rates were noticeably distinct, the lower one
428 recovering more rapidly.
429
430 Further down the slope, at L4, the two tensiometers (Fig. 9 b), positioned at 25 cm and 80 cm
431 below the ground surface; and the water level in the groundwater observation holes (Fig. 9 a),
432 all responded in a uniform, simultaneous and similar pattern to the rainfall events that
433 occurred between the beginning of the season to about mid-February, when the water level
434 seemed to have reached the ground surface. This implies a rapid propagation of a pressure
435 wave through the soil profile at this observation nest (L4). It is necessary to point out that,
436 when a rainfall event of high intensity and magnitude impinged the ground surface, with the
437 subsurface conditions of a deep water table and a dry soil profile above, the responses of pore
438 water pressure and water level were relatively rapid and large in magnitude. This was
439 particularly noticeable, for instance, during the rainfall events 19 and 54, which occurred on
440 8th November 2000 and 28th January 2001, respectively. A critical consideration of the
441 responses of the water level and tensiometric pore water pressure at L3 and L4 indicates that,
442 the water level responses at L3 followed more, although with some lag time, into the pattern
443 of water level responses at L4, than in the pattern of its counterpart tensiometers at L3. This
444 phenomenon was again more evident during the rainfall events 19 and 54. It will suffice to

445 present in detail just one of these two events, Event 19, of which the results, are shown in Fig.
446 8.
447
448 In Fig. 10(a) the water levels were plotted with bedrock, as a zero datum. The geology of this
449 zone indicates that the bedrock gradient dips from L2 and L4, converging at L3 (see Fig. 2).
450 This configuration of the bedrock topography explains the presence of 40 cm of water in the
451 observation hole at L3 and the absence of water in the observation hole at L4, in the pre-event
452 period of Event 19 (Fig. 10a). Since the gradient of bedrock between L4 and L3 is small, a
453 horizontal bedrock datum was assumed, from which the water levels in Fig. 10 were plotted.
454
455 At L4, before Event 19, the tensiometer at 25 cm and 80 cm below the ground surface
456 indicated the pre-event pressure potential values of about 70 cm-H_2O and 45 cm-H_2O,
457 respectively (Fig. 10b), while the observation hole indicated dry conditions (Fig. 10a).
458
459 During Event 19, the middle tensiometer at L3 (tens @ 50 cm) reacted rapidly, while the
460 deeper tensiometer (tens @ 80 cm) did react only slightly. At L4, the pore water pressure at
461 the two tensiometers and the water levels started to react at 16h35, 2 minutes after the peak
462 rainfall intensity impinged the ground surface (Table 2). Given that the logging time
463 resolution of the data was 12 minutes, the lag time between the peak rainfall intensity and the
464 responses of the tensiometric pore water pressure and the water level might have been less
465 than 2 minutes. The deeper tensiometer recorded a change of 110.4 cm-H_2O in the soil pore
466 water pressure, while the water level was elevated by 106.1 cm; both within two-and-a-half
467 hours, but the former reacting more slowly than the latter. This simultaneous and almost
468 equivalent magnitude of the change in the water level and the tensiometric pore water
469 pressure indicates signals of the Lisse Effect pressure wave. Torres *et al.* (1998) observed a

similar simultaneous response in tensiometric pore water pressure at different soil depths and two different observation points, when they applied intense irrigation rates (between 370 and 5725 mm/h) on the ground surface. Torres *et al.* (1998) speculated compressed pore air ahead of the wetting front (Lisse Effect).

3.3 Laboratory Experimental Results

In the pre-simulation period, in the laboratory experiment, all the tensiometers indicated unsaturated conditions (negative pressure potential). The pre-simulation piezometric water level was at Port 160, which corroborates with the pressure potential value at this port (0 pressure head). However, the volumetric water content at Port 160 and Port 150 indicated maximum saturation, while Port 140 indicated partially saturated conditions. Therefore, from the tensiometric pore water pressure, volumetric water content and pore air-entry value of the soil used (Table 1), Port 160 was on the water table, Port 150 was right in the middle of the capillary fringe and Port 140 was close to the upper boundary of the capillary fringe.

During the simulation, pore air pressure, tensiometric pore water pressure and piezometric water levels responded, as soon as water was ponded on the soil surface. The volumetric water content of the shallowest sensor, i.e., Port 60, responded almost 44 minutes after the start of the experiment (Fig. 11). These observations indicate that the tensiometric pore water pressure and piezometric water levels responded to the compressed pore air pressure, before the arrival of the wetting front. The decrease in the volumetric water content at Port 140 and Port 150, were caused by groundwater depletion, as a result of groundwater discharge (results not shown).

494 The rise in the piezometric water level was nearly always on a par with the increase in the
495 fluid pressure in the soil pore water (ψ) inside the column, as indicated by the tensiometer at
496 Port 160. The increase in ψ was proportional to the increase in compressed pore air. It is also
497 worth noting that, the tensiometers, which were above the water table, reacted from their
498 initial more-negative pressure potential values to their less-negative pressure potential values
499 in a gradual manner.
500

501 **4. Discussion**

502 **4.1 The role of the capillary fringe in the transient pressure waves**

503 *The Lisse effect transient pressure wave*

504 Results from the hillslope zone showed that, in the pre-event period of Event 19, there was
505 completely no water in the observation hole at L4. Conversely, during Event 19, it was noted
506 that there were rapid and disproportionate responses in tensiometric pore water pressure, as
507 well as the water level at L4. The rapidly elevated pore water pressure and water level
508 remained at their new elevated values, for several days, after the rainfall event (Fig. 10). This
509 phenomenon is the Lisse Effect, which is described as: "initially rapid, 2-4 days for full
510 recovery," (Heliotis and DeWitt, 1987, Table 1).
511

512 In the pre-event period of Event 19, there was 40 cm of water above the bedrock in the
513 observation hole at L3. From the water levels at L3 and L4, and the configuration of the
514 bedrock topography, the profiles of the water table and the capillary fringe, between the two
515 nests and prior to Event 19, can be extrapolated, as shown in Fig. 12. With Fig. 12, the
516 processes that occurred at L4 can be explained clearly with the aid of the laboratory results.
517

The laboratory results revealed that the Lisse Effect water table response is mainly caused by the release of tension forces in water within the capillary fringe, and that the total rise in the piezometric water level was caused by the cumulative effect of two main processes. First, the pressure energy injected into the capillary fringe, due to the compressed pore air pressure, releases the tension forces in the water within the capillary fringe, hence subjecting it (water within the capillary fringe) to gravity forces. This elevates the hydraulic head that results in the initial rapid rise of the piezometric water level (see Fig. 13 a, b, and c). Secondly, if the injected pressure energy is significantly large, the excess pressure energy adds to the already raised hydraulic head (caused by the first process) (see Fig. 13 d). The first process explains the sudden appearance of water in the observation hole at the field's observation nest L4. The downward pressure wave increased the fluid pressure in the water within the capillary fringe (Fig. 12), hence, rapidly causing the effusion of the stored pre-event water as it (pressure wave) propagated downward. The effused pre-event water accounts for the sudden appearance of water in the observation tube, which was dry in the pre-event period of the rainfall Event No. 19. Similar processes of the conversion of the capillary fringe (as shown in Fig. 13) occurred at the observation nest U3, at the wetland zone.

Groundwater ridging transient pressure wave

Field results from the observation nest U3, at the wetland zone, revealed that groundwater ridging occurred only in the rainfall events that had a minimum total rainfall depth of 10 mm (Fig. 6)). The point of discussion here is that this threshold amount also depends on the position of the tensiometer, within the capillary fringe, or below the ground surface. For instance, had the tensiometer been in a shallower position, the value of the minimum total rainfall amount could have been higher, and vice-versa. However, the minimum total rainfall amount suggests that, in a given suitable environment, any small amount of water can not

cause groundwater ridging, as indicated by Gillham (1984); instead, a threshold amount is required. Our observations, on the other hand, support those of Heliotis and DeWitt (1987), who found that a critical amount of rainfall was required to cause a rapid water table response.

An interesting feature was identified in the pressure curves of the shallower tensiometer at U3. The pressure curves indicated a more rapid reaction of the tensiometer, before the zero pressure-head value, than after the zero pressure-head value. This feature, according to the law of conservation of energy, implies an onset of lateral flow of water below the rising water table. We discuss this feature with reference to Fig. 14, which was developed from Fig. 8(a).

Fig. 14 (a) represents the state of the system in the pre-event period. The shallower tensiometer indicated negative pressure potential (-27.2 cm-H_2O), while the deeper tensiometer indicated positive pressure potential (56.5 cm-H_2O). However, from the soil water retention information (h_a = 45 cm-H_2O, Table 1), the shallower tensiometer was within the capillary fringe, which extended to the ground surface, as idealized in Fig. 14(a). It is important to keep in mind that the water within the capillary fringe is usually under tension forces and cannot flow by gravity. Only the water below the water table can flow by gravity.

Fig. 14 (b) represents the state of the system, during the initial period of the rainfall event. Since the capillary fringe is saturated, no infiltration of the rainwater is anticipated. Therefore, formation of saturated overland flow (SOF), or ponding, is expected at the on-set of a rainfall event. The impact of rainfall on the ground surface (Arrow A) and the ensuing SOF, or ponding, (Arrow B) injects positive pressure into the soil profile (the capillary fringe). This injected pressure energy propagates through the capillary fringe, as a downward pressure wave (Arrow C), releasing tension pressure in water within the capillary fringe. As soon as

568 the initial downward pressure wave-front arrives on the water table, the water table starts to
569 ascend, as shown in Fig. 14 (c) (Arrow D). The water that was initially under tension, within
570 the capillary fringe, is now under positive pressure and subjected to gravity flow, below the
571 rising water table. As the water table rises, therefore, the converted water, underneath the
572 water table, flows laterally, as shown in Fig. 14 (c) (Arrow E). Consequently, due to this
573 lateral flow, the rate of the rising water table (upward pressure wave) would be lower than the
574 rate of the downward pressure wave, a phenomenon that results in the decrease in the rate of
575 response of the pressure curve, after crossing the zero pressure line (Fig. 8a). For
576 completeness, where there is no provision for lateral flow, the refraction in the pressure curve
577 at zero pressure head is expected not to occur.
578
579 **4.2 Response of groundwater fluxes at a hillslope zone**
580 The response in the water level at L3, located in the upslope of L4, occurred, after the
581 response in the water level at L4, located near the toe of the slope. This delayed water level
582 response at L3 is caused, neither by the recharge of the water table from the infiltration
583 profile, nor by the subsurface groundwater flow from the upslope direction. This is based on a
584 number of reasons. Although, as it has been mentioned above, there seem to be preferential
585 flows at L3, the infiltration profile through this mechanism (preferential flows) did not reach
586 the deeper soil horizon, to recharge the water table. This is from the lack in response of the
587 deeper tensiometer at L3 (Fig. 10c). Furthermore, since no change was recorded in the water
588 level at L2 (Fig. 9), the rapid response of the water level at L3 was not caused by the
589 groundwater flow from the upslope direction. Therefore, the rapid response of the water level
590 at L3 was caused by the reversed groundwater flow from the downslope direction, after the
591 rapid elevation of the hydraulic head in groundwater at the toe of the slope (L4).
592

593 The general direction of groundwater fluxes between L3 and L4 at any time was determined
594 from the hydraulic gradient between the two nests. In Fig. 15, the hydraulic grade lines are
595 shown for five specific times, during and immediately after Event 19. The hydraulic grade
596 lines in Fig. 15 were plotted by joining the hydraulic heads between L3 and L4 at the
597 specified times. The value of the hydraulic gradient for each hydraulic grade line for the
598 specified times are also indicated in Fig. 15.
599
600 Just before the rapid response of the water level at L4, to the peak rainfall intensity, which
601 occurred at 16h33, the hydraulic gradient between L3 and L4 was 0.0100, towards the
602 downslope direction (Fig. 15). Immediately the peak intensity rainfall impinged the ground
603 surface, the water level at L4 (right hand vertical axis of Fig. 15) was rapidly elevated,
604 attaining the maximum change of 106 cm in two hours, and of which 90 cm was recorded in
605 the initial 24 minutes. On the other side (left hand vertical axis of Fig. 15), the water level at
606 L3 did not immediately respond to this intense rainfall, except for a small rise of about 3 cm
607 that might have been caused by a shock or vibration wave (Amiaz *et al.*, 2011). Therefore,
608 due to the rapid increase of the difference in fluid pressures between the two nests, there was
609 about 205 % (181.2^{o}) overturn in the hydraulic gradient from 0.0100, in the downslope
610 direction, to 0.0105, in the upslope direction, in just 24 minutes. The overturned hydraulic
611 gradient consequently caused an overturn in the direction of groundwater fluxes. The
612 overturning wave, which developed and attained a pressure potential of 90 cm-H_2O at L4 at
613 16h59 on the 8th November; arrived at L3, 46 m in the upslope direction, on the 9th
614 November 16h23, almost 24 hours later, with an attenuated pressure potential of 31 cm-H_2O.
615

4.3 The role of transient pressure wave water table responses in stream generation

The results presented in this paper adds to the numerous proposed answers (e.g. Bishop *et al.*, 2004), to the questions that have been raised, regarding the storage of the pre-event water in a catchment and its subsequent rapid mobilization during a rainfall event (Kirchner, 2003). The results from the present study support earlier arguments (e.g. Buttle, 1994) that, in the pre-event period, a substantial amount of pre-event water is stored in an immobilized form, within the capillary fringe. During a rainfall event, this stored pre-event water may be rapidly mobilized by, either the groundwater ridging or the Lisse Effect. Furthermore, the pre-event water, stored in the capillary fringe, due to its proximity to the ground surface, is chemically and isotopically distinct from the pre-event water, stored under the phreatic surface and forms the baseflow (Buttle, 1994). Therefore, when the pre-event water within the capillary fringe is mobilized into the stream, it introduces an isotopic and a chemical signature that is distinct from that of the new event water, derived from the rainfall event, as well as the pre-event water, derived from the baseflow (groundwater). The stormflow hydrograph, therefore, may consist of three chemically and isotopically distinct types of water (Ogunkoya and Jenkins, 1993).

The results presented in this study demonstrate that the groundwater ridging and the Lisse Effect are among the predominant mechanisms responsible for mobilization of pre-event water from hillslopes to the stream in the Weatherley research catchment. This supports the findings of Wenninger *et al.* (2008), who observed that even during flood events; groundwater component formed at least 62% of the total event runoff.

5. Conclusion and Further Research Work

Groundwater ridging transient pressure wave mechanism occurs, where and when the capillary fringe is very close to, or intersects, with the ground surface.

Groundwater ridging mechanism can rapidly mobilize pre-event water from the soil profile and account for its (pre-event water) significant appearance in the stream stormflow hydrograph. This conclusion is made from field observations and should, therefore, serve to alleviate any skepticism, regarding the practicability of groundwater ridging in the field conditions.

Owing to the characteristics of the capillary fringe, or the zone of tension saturation, any small amount of water introduced on the ground surface, in an environment that is suitable for groundwater ridging, cannot cause a rapid water table response. Instead, the groundwater ridging water table response depends on the intensity, with which water is applied on the ground surface. The applied water intensity introduces additional energy, which releases tension forces in water within the capillary fringe, hence, enabling the water table to rise. Therefore, the total water response, in the groundwater ridging mechanism, is proportional to the intensity of rainfall.

The capillary fringe plays a central role, not only in the groundwater ridging, but also in the Lisse Effect. In both mechanisms, the water table responses occur, as a result of an introduction of additional energy into the capillary fringe. In the groundwater ridging, due to the proximity of the capillary fringe to the ground surface, an additional energy is derived directly from the rainfall intensity. In the Lisse Effect, the additional energy is derived from compressed pore air, in the unsaturated zone and ahead of a wetting front.

664

665 In both mechanisms, the introduced energy propagates towards the water table, as a
666 downward pressure wave, releasing tension forces in water within the CF. As soon as the
667 downward pressure wave front arrives on the water table (WT); the WT begins to ascend, as
668 an upward pressure wave. The ascending WT contributes to the pressure potential in
669 groundwater, hence elevating the hydraulic head, which disproportionately increases the
670 groundwater fluxes.

671

672 Further studies are recommended to develop a mathematical theory for the physical processes
673 involved in groundwater ridging and the Lisse Effect water table responses.

674

675 **6. Acknowledgements**

676 The first author is a PhD student, who is funded by the Germany Academic Exchange Service
677 (DAAD). Field and laboratory studies were funded by the Water Research Commission of
678 South Africa. This study is hosted by the School of Engineering and the Centre for Water
679 Resources Research (CWRR), University of KwaZulu-Natal (UKZN); and supported by the
680 Department of Soil, Crop and Climate Sciences (SCCS), University of the Free State (UFS);
681 South Africa. Mr. JJ Pretorius, Chief Technician at the SE and CWRR, provided technical
682 advice. English language was edited by Dr Sharon Rees of the SE and CWRR, UKZN. Two
683 anonymous reviewers made valuable comments on the initial manuscript. Every support
684 received from each organization, institution and individual is acknowledged and appreciated.

685

686 **7. References**

687 Abdul, A.S., Gillham, R.W. 1984. Laboratory studies of the effects of the capillary fringe on
688 streamflow generation. Water Resour. Res. 20(6), 691-698.

689 Abdul, A.S., Gillham, R.W. 1989. Field studies of the effects of the capillary fringe on
690 streamflow generation. J. Hydrol. 112(1-2), 1-18.
691 Adrian, D.D., Franzini, J.B. 1966. Impedance to infiltration by pressure build-up ahead of the
692 wetting front. J. Geophys. Res. 71(24), 5857-5862.
693 Amiaz, Y., Sorek, S., Enzel, Y., Dahan, O. 2011. Solute transport in the vadose zone and
694 groundwater during flash floods. Water Resour. Res. 47(10), W10513.
695 Bishop, K., Seibert, J., Köhler, S., Laudon, H. 2004. Resolving the double paradox of rapidly
696 mobilized old water with highly variable responses in runoff chemistry. Hydrol.
697 Process. 18(1), 185-189.
698 Bond, W.J., Collis-George, N. 1981. Ponded infiltration into simple soil systems: 3. The
699 behavior of infiltration rate with time. Soil Sci. 131(6), 327-333.
700 Brooks, R.H., Corey, A.T. 1964. Hydraulic properties of porous media. Colorado State
701 University, Fort Collins, CO, 27 pages.
702 Brooks, R.H., Corey, A.T. 1966. Properties of porous media affecting fluid flow. J. Irrig.
703 Drain. Div., ASCE 92(IR2), 61-88.
704 Burns, D.A., Plummer, L.N., McDonnell, J.J., Busenberg, E., Casile, G.C., Kendall, C.,
705 Hooper, R.P., Freer, J.E., Peters, N.E., Beven, K. 2003. The geochemical evolution of
706 riparian ground water in a forested piedmont catchment. Ground Water 41(7), 913-
707 925.
708 Buttle, J.M. 1994. Isotope hydrograph separations and rapid delivery of pre-event water from
709 drainage basins. Prog. Phys. Geog. 18(1), 16-41.
710 Buttle, J.M., Sami, K. 1992. Testing the groundwater ridging hypothesis of streamflow
711 generation during snowmelt in a forested catchment. J. Hydrol. 135(1-4), 53-72.
712 Free, G.R., Palmer, V.J. 1940. Interrelationship of infiltration, air movement, and pore size in
713 graded silica sand. Soil Sci. Soc. Amer. Proc. 5390-398.

714 Freeze, R.A., Cherry, J.A. 1979. Groundwater. Prentice-Hall, Englewood Cliffs, New Jersey.
715 Gee, G.W., Bauder, J.W. 1986. Particle-size analysis, in: Klute, A. (Eds.), Methods of soil
716 analysis. Part 1. Physical and mineralogical methods. American Society of Agronomy,
717 Madison, Wisconsin, 383–411.
718 Gillham, R.W. 1984. The capillary fringe and its effect on water-table response. J. Hydrol.
719 67(1-4), 307-324.
720 Heliotis, F.D., DeWitt, C.B. 1987. Rapid water table response to rainfall in a Northern
721 Peatland ecosystem. Water Res. Bull. 23(6), 1011-1016.
722 Jayatilaka, C.J., Gillham, R.W. 1996. A deterministic-empirical model of the effect of the
723 capillary fringe on near-stream area runoff 1. Description of the model. J. Hydrol.
724 184(3-4), 299-315.
725 Jayatilaka, C.J., Gillham, R.W., Blowes, D.W., Nathan, R.J. 1996. A deterministic-empirical
726 model of the effect of the capillary fringe on near-stream area runoff 2. Testing and
727 application. J. Hydrol. 184(3-4), 317-336.
728 Khaled, I.M., Kohei, N., Taku, N., Hiromi, I., Tsuyoshi, M. 2007. Laboratory investigations
729 of short-term fluctuations of shallow groundwater in response to recharge events.
730 Khaled, I.M., Tsuyoshi, M., Kohei, N., Taku, N., Hiromi, I. 2011. Experimental and modeling
731 investigation of shallow water table fluctuations in relation to reverse Wieringermeer
732 effect. Open Journal of Soil Science 1(2), 17-24.
733 Kirchner, J.W. 2003. A double paradox in catchment hydrology and geochemistry. Hydrol.
734 Process. 17(4), 871-874.
735 Klute, A. 1986. Water retention: Laboratory methods, in: Ed. Klute, A. (Eds.), Methods of
736 soil analysis. Part 1. Physical and mineralogical methods. American Society of
737 Agronomy, Madison, Wisconsin, 635-662.

738 Klute, A., Dirksen, C. 1986. Hydraulic conductivity and diffusivity: Laboratory methods, in:
739 Klute, A. (Eds.), Methods of soil analysis. Part 1. Physical and mineralogical methods.
740 American Society of Agronomy, Madison, Wisconsin, 687-734.
741 Lorentz, S.A., Thornton-Dibb, S., Hickson, R., Sihlophe, N. 2001. Hydrological systems
742 modelling research programme: Hydrological processes: Phase I Processes definitions
743 and database. Water Research Commission, Pretoria.102 pp.
744 Lorentz, S.A., Thornton-Dibb, S., Pretorius, C., Goba, P. 2004. Hydrological systems
745 modelling research programme: Hydrological processes: Phase II Quantification of
746 hillslope, riparian and wetland processes. 1061 & 1086/1/04. Water Research
747 Commission, Pretoria.130 pp.
748 McDonnell, J.J. 1990. A rationale for old water discharge through macropores in a steep,
749 humid catchment. Water Resour. Res. 26(11), 2821–2832.
750 McDonnell, J.J., Buttle, J.M. 1998. Comment on "A deterministic--empirical model of the
751 effect of the capillary-fringe on near-stream area runoff. 1. Description of the model"
752 by Jayatilaka, C. J. and Gillham, R. W. (Journal of Hydrology vol. 184 (1996) 299-
753 315). J. Hydrol. 207(3-4), 280-285.
754 McWhorter, D.B. 1971. Infiltration affected by flow of air. Hydrol. Pap. 49. Colo. State Univ.
755 Fort Collins, Colorado, USA.
756 Ogunkoya, O.O., Jenkins, A. 1993. Analysis of storm hydrograph and flow pathways using a
757 three-component hydrograph separation model. J. Hydrol. 142(1), 71-88.
758 Peck, A.J. 1960. The water table as affected by atmospheric pressure. J. Geophys. Res. 65(8),
759 2383-2388.
760 Pinder, GF, Jones, JF. 1969. Determination of the ground-water component of peak discharge
761 from the chemistry of total runoff. Water Resour. Res. 5(2), 438-445.

762 Rasmussen, T.C., Baldwin Jr, R.H., Dowd, J.F., Williams, A.G. 2000. Tracer vs. pressure
763 wave velocities through unsaturated saprolite. Soil Sci. Soc. Am. J. 64(1), 75-85.
764 Sklash, MG, Farvolden, RN. 1979. The role of groundwater in storm runoff. J. Hydrol. 43(1-
765 4), 45-65.
766 Torres, R., Dietrich, W.E., Montgomery, D.R., Anderson, S.P., Loague, K. 1998. Unsaturated
767 zone processes and the hydrologic response of a steep, unchanneled catchment. Water
768 Resour. Res. 34(8), 1865-1879.
769 Touma, J., Vachaud, G., Parlange, J.Y. 1984. Air and water flow in a sealed, ponded vertical
770 soil column: experiment and model. Soil Sci. 137(3), 181-187.
771 Wang, Z., Feyen, J., van Genuchten, M.T., Nielsen, D.R. 1998. Air entrapment effects on
772 infiltration rate and flow instability. Water Resour. Res. 34(2), 213-222.
773 Weeks, E.P. 1979. Barometric fluctuations in wells tapping deep unconfined aquifers. Water
774 Resour. Res. 15(5), 1167-1176.
775 Weeks, E.P. 2002. The Lisse Effect revisited. Ground Water 40(6), 652-656.
776 Wenninger, J., Uhlenbrook, S., Lorentz, S.A., Leibundgut, C. 2008. Identification of runoff
777 generation processes using combined hydrometric, tracer and geophysical methods in
778 a headwater catchment in South Africa. Hydrol. Sci. J. 53(1), 65-80.
779 Wenninger, J., Uhlenbrook, S., Tilch, N., Leibundgut, C. 2004. Experimental evidence of fast
780 groundwater responses in a hillslope/floodplain area in the Black Forest Mountains,
781 Germany. Hydrol. Process. 18(17), 3305-3322.
782
783
784
785
786
787

TABLES

Table 1. The physical properties of the soils at the selected observation nests (obtained from Lorentz *et al.*, 2001) and of the soil used in the laboratory experiments.

Site	Depth (m)	K_s (cm/h)	h_a (cm)	Soil texture	Porosity	Density (Kg/m^3)	*CS (%)	*MS (%)	*FS (%)	*S&C (%)
L2	0.00	38.81	39.20	SaLm	0.37	1750				
	0.40	3.97	21.46	SaLm	0.33	1775				
	0.80		49.75	SaLm	0.30	1850				
L3	0.00	32.94		SaLm						
	0.50	3.97	10.14	SaLm	0.32	1791				
	0.70		0.61	Lm	0.34	1760				
	1.50		71.94	ClLm	0.30	1871				
L4	0.00	29.24		SaLm						
	0.20	0.50	78.74	SaLm	0.286	1892	18.3	29.0	42.4	10.2
	0.50	0.72	8.70	SaLm	0.352	1717	21.8	26.3	44.7	7.2
	0.90	0.72		SaSiCL			23.8	30.3	41.0	4.8
*U3	0.00-0.40	2.35	45	SaLm		1818	12.9	16.4	36.5	34.1
	0.40-0.80	11.32		SaLm		1410				
U4	0.00			ClLm	0.468	1410				
	0.20			ClLm	0.428	1516				
*Lab	0-1.7	45	20	Sa	0.44	1500	26.0	72.0	2.0	

K_s = Saturated hydraulic conductivity, h_a = pore air entry pressure head, CS = coarse sand (0.50 – 2.00 mm), MS = medium size sand (0.25 – 0.50 mm), FS = fine sand (0.053 – 0.25 mm), S&C = Silt & Clay (< 0.053 mm). *Data determined during the present study.

Table 2. Rainfall events that caused rapid water table responses in the Weatherley research catchment during the summer season of 2000/2001.

Event No.	Start time yyyy/mm/dd/ hh:mm	End time yyyy/mm/dd/ hh:mm	Event duration (h m)	Total rainfall (mm)	Max. 1-min intensity (mm/h)	Time of max intensity (hh:mm)
	2000/11/					
19	08/15:41	08/18:42	1h 24m	67.8	228	16:33
20	12/16:38	12/16:55	0h 18m	4.6	60	16:42
22	18/10:40	18/23:43	13h 03m	11.4	24	17:51
28	28/13:43	28/18:36	4h 53m	16	84	13:56
	2000/12/					
32	03/14:32	03/17:51	3h 19m	10.8	66	14:39
34	07/17:32	07/23:58	6h 26m	12.4	18	19:14
36	10/13:09	11/22:32	33h 23m	42.8	24	13:16
38	20/17:22	20/20:37	3h 15m	29.4	78	18:34
39	24/13:59	25/14:35	24h 36m	31.2	90	16:47
	2001/01/					
42	01/00:01	02/06:53	30h 52m	27	30	7:07
43	08/13:50	08/23:04	9h 14m	20	18	21:00
46	13/14:06	14/11:08	21h 02m	28	84	88:12
47	18/18:04	18/19:41	1h 37m	11.2	30	18:15
48	19/15:50	19/21:11	5h 21m	4.6	12	15:57
49	20/15:37	20/15:55	0h 18m	6.8	48	15:43
54	28/12:07	29/00:58	12h 51m	39.8	42	12:52
	2001/02					
58	07/17:42	07/20:39	2h 57m	15	48	17:56
60	13/16:40	15/04:51	36h 11m	56.4	60	17:21
62	19/15:56	19/20:10	4h 14m	16.2	84	16:00
65	23/13:51	23/21:26	7h 35m	21.8	48	14:51
	2001/03/					
70	10/13:16	10/20:28	7h 12m	47.2	102	14:05
75	17/14:10	17/19:24	5h 14m	26.6	132	15:32
80	23/16:45	23/22:19	5h 34m	17.6	66	16:37
	2001/04/					
88	08/19:31	08/20:48	1h 17m	8.6	66	20:40
89	10/19:08	10/19:38	0h 30 m	32	156	19:25
93	23/18:47	23/22:31	3h 44m	12.6	90	20:32

Table 3. Rainfall events, in which the water table response to groundwater ridging transient pressure wave occurred at the observation nest U3. The pre-event water table (WT) was estimated from the pressure potential (PP) values of the deeper tensiometer.

Col.1	Col.2	Col.3	Col.4	Col.5	Col.6	Col.7	Col.8	Col.9
Rainfall				**Response of the shallower (Tens @ 20 cm)**			***Pre-event WT below ground surface (cm)**	**Days from previous event with rainfall >10 mm**
Event No.	**Start time yyyy/mm/ dd/hh:mm**	**Total depth (mm)**	**Max. intensity (mm/h)**	**Start PP (cm-H_2O)**	**End PP (cm-H_2O)**	**Total (cm-H_2O)**		
	2000/11/							
28	28/13:43	16	84	-23.85	15.68	39.53	32.54	19.86
	2000/12/							
32	03/14:32	10.8	66	-1.30	8.72	10.02	23.63	4.83
34	07/17:32	12.4	18	-10.49	12.06	22.55	26.97	3.99
38	20/17:22	29.4	78	-20.80	17.08	37.88	34.50	8.78
39	24/13:59	31.2	90	-2.14	20.70	22.84	18.90	3.72
	2001/01/							
42	01/00:01	27	30	-9.38	15.12	24.50	23.40	6.39
43	08/13:50	20	18	-27.20	12.62	39.82	43.40	6.29
46	13/14:06	28	84	-24.41	15.96	40.37	40.89	4.63
47	18/18:04	11.2	30	-18.29	9.83	28.12	31.43	4.29
	2001/02/							
60	13/16:40	56.4	60	-5.20	27.38	32.88	20.85	5.83
	2001/03/							
70	10/13:16	47.2	102	-23.57	30.44	54.01	39.22	14.66

866 **LIST OF FIGURE CAPTIONS**

867 Fig.1. (a) The Weatherley research catchment and (b) its location in South Africa (from
868 Lorentz *et al.*, 2001).

869 Fig. 2. Positions of the tensiometers and groundwater observation holes (GWOH) in the soil
870 profile at the raised hillslope zone (vertical scale is exaggerated 4 times). *i* =
871 observation nest; *j* = tensiometer number; OH = groundwater observation hole; t_{ij} =
872 tensiometer number *j* below the ground surface and at the observation nest L*i;* and
873 OH_i is the groundwater observation hole at observation nest L*i*.

874 Fig. 3. Schematic presentation of the pore-air pressure probe.

875 Fig. 4. The initial conditions (pre-simulations conditions) for the laboratory experiment. θ_r =
876 residual soil water content, θ_s = saturated soil water content.

877 Fig. 5. The response of (a) the stream discharge over the upper weir, (b) the tensiometric
878 pore water pressure at U3 and (c) the tensiometric pore water pressure at U4 to (d)
879 the daily rainfall during the summer season of 2000/2001. The stream discharge axis
880 in (a) is truncated at 100 m^3/h. The values on the discharge curve are the respective
881 temporal maximum flow rate for discharges > 100 m^3/h.

882 Fig. 6. The influence of peak rainfall intensity and total rainfall depth on the water table
883 response to groundwater ridging (GWR) transient pressure wave at U3.

884 Fig. 7. General linear relationship between events' peak rainfall intensities and the total
885 changes in pore water pressure within the capillary fringe (at the shallower
886 tensiometer) during the groundwater ridging transient pressure waves at U3. The R^2
887 of 0.9084 is achieved, when the three crossed events are excluded. In the three
888 events, the tensiometer recorded the most extreme values of pre-event pressure
889 potential; the upper two events had the highest values, while the lower single event
890 had the lowest value (see Table 2.3, Col. 5).

891 Fig. 8. The responses of the tensiometers at U3 to (a) the rainfall Event No. 43 that
892 occurred on 8th January 2001 and (b) the rainfall Event No. 70 that occurred on 10th
893 March 2001. PP is pressure potential.
894 Fig. 9. Responses of the water levels in the groundwater observation holes (GWOH) and
895 tensiometric pore-water pressure at observation nests L2, L3 and L4 to daily rainfall
896 during the summer season of 2000/2001. Missing data was caused by mechanical
897 breakdown in the logging system.
898 Fig. 10. The responses of the water levels in groundwater observation holes (GWOH) and the
899 tensiometric soil pore water pressure at observation nests L3 and L4 to rainfall Event
900 No. 19.
901 Fig. 11. The responses of (a) the piezometric water level, tensiometric pore water pressure
902 and compressed pore-air pressure, and (b) volumetric soil water content during the
903 laboratory experiment. The results in (a) are only for the first 5 minutes and those in
904 (b) are for the first 120 minutes of the experiment.
905 Fig. 12. Extrapolated profiles of the water table and the capillary fringe between L3 and L4,
906 prior to the rainfall Event No. 19. The extrapolation is based on the water level at L3
907 (40 cm) and at L4 (0 cm), prior to the event, and the topography of the bedrock. The
908 vertical scale is exaggerated four times.
909 Fig. 13 Temporal and discrete evolution of the water table (WT) caused by the release of
910 tension forces in water within the capillary fringe (CF) in the Lisse Effect laboratory
911 experiment. The arrow on top of the CF represents the compressed pore air in the
912 unsaturated zone (UZ), the downward arrow within the CF represents positive
913 pressure propagating downwards (downward pressure waves) towards the water table
914 (WT) and the upward arrow represents the rising WT (upward pressure wave).
915 Time, *t*, is in minutes and with reference to Fig. 11. (a) is before the start of

916 experiment, (b) is the downward pressure wave through capillary fringe, but just
917 before it arrives on the WT, (c) the WT through capillary fringe, (d) the WT has just
918 arrived on top of the CF and (e) the water level in the piezometer rises above the top
919 of the saturated zone inside the column of soil (this is caused by the excess
920 compressed pore air).

921 Fig. 14. Schematic presentation of (b) the release of tension forces in water within the
922 capillary fringe, (c) the subsequent rising water table and the simultaneous lateral
923 flow of water, below the rising water table, during groundwater ridging water table
924 response. (a) is the pre-event state. Arrows: A = rainfall, B = saturated overland flow,
925 C = downward pressure wave through capillary fringe, D = rising water table
926 (upward pressure wave), E = ensuing lateral flow, as the negative pressure in the
927 water within the capillary fringe is turned into positive pressure, F = pressure wave,
928 under the water table (and due to the rising water table), propagating toward the
929 deeper tensiometer. WT = water table, IWT = initial water table. The three states
930 (times) of the water table are with reference to Figure 2.8(a).

931 Fig. 15. The temporal and discrete evolution of the hydraulic gradient between L3 and L4, as
932 a result of a transient pressure wave at L4 during the rainfall Event No. 19.

933

934

935

 doi:10.2136/vzj2012.0054

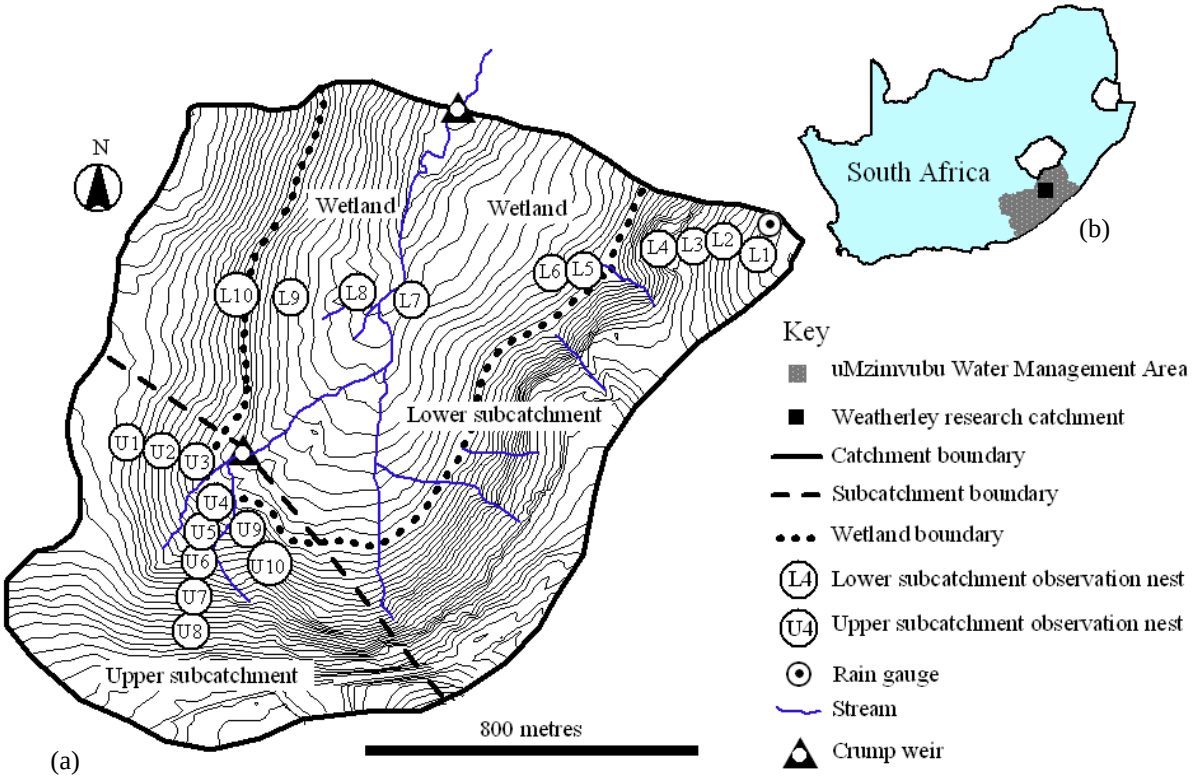

 doi:10.2136/vzj2012.0054

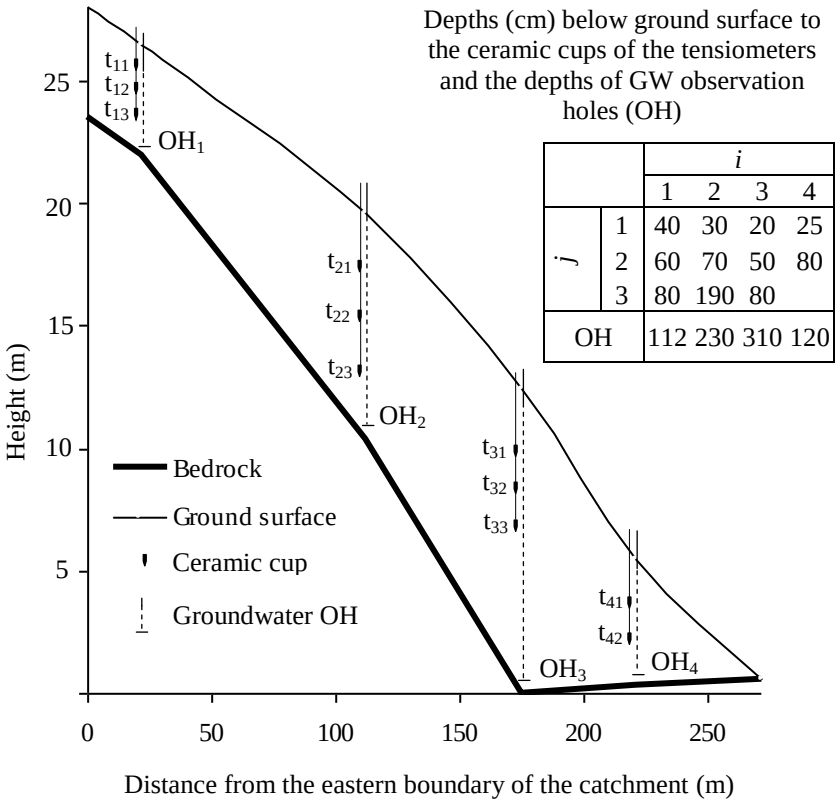

 doi:10.2136/vzj2012.0054

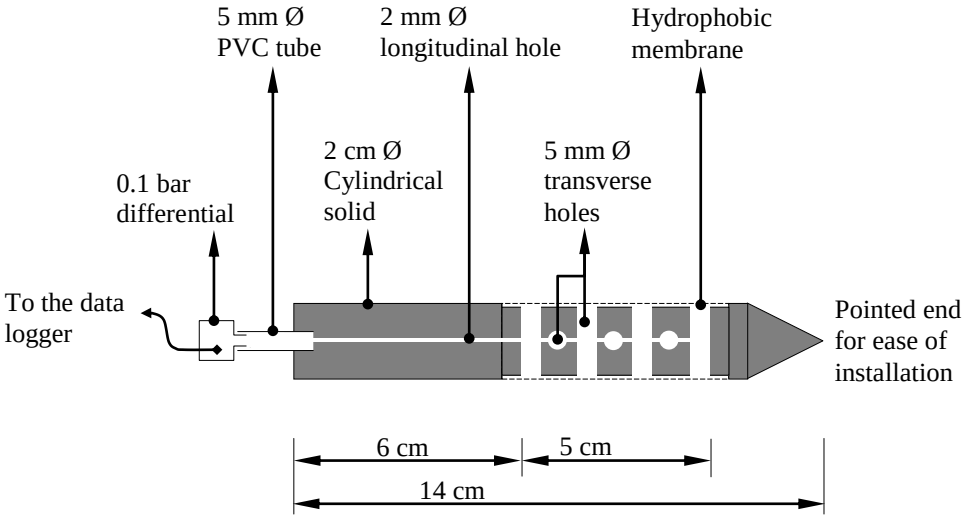

 doi:10.2136/vzj2012.0054

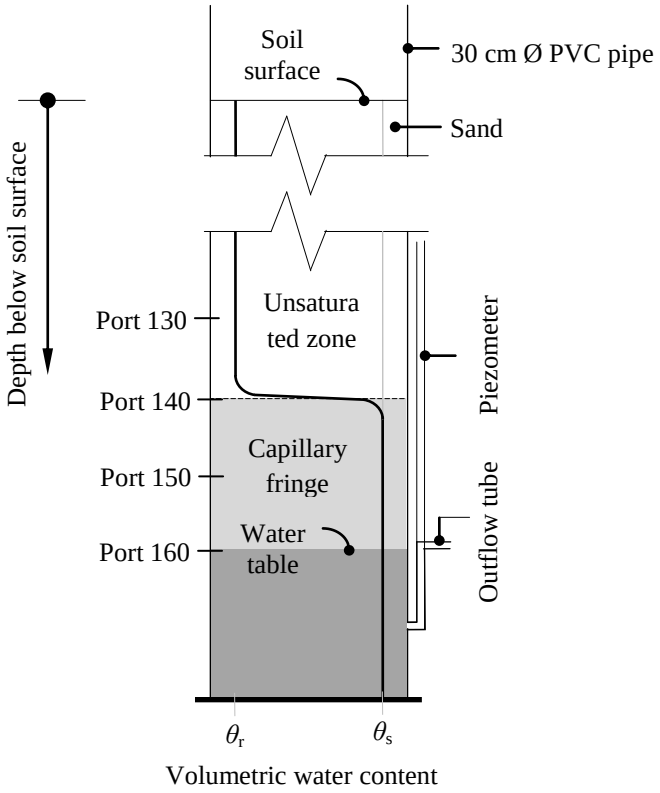

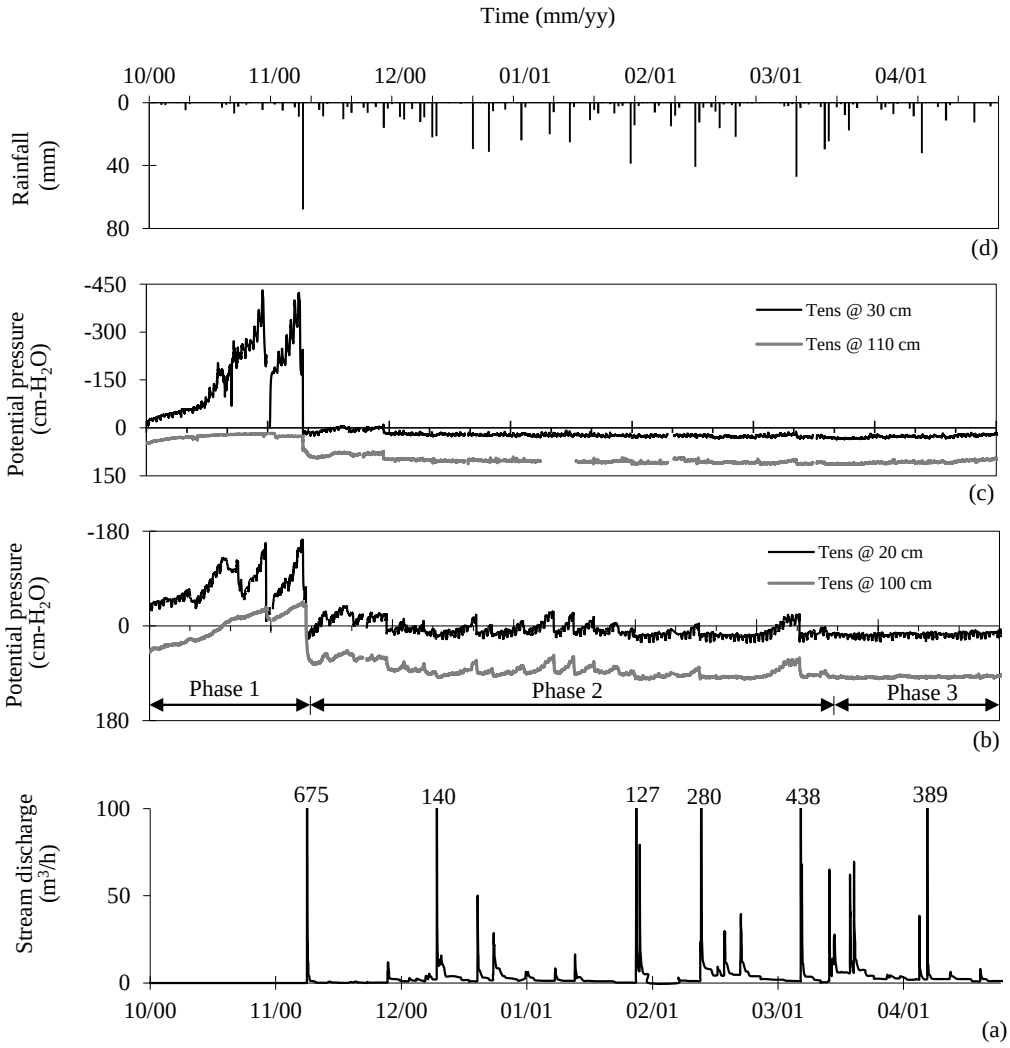
Time (mm/yy)
10/00
11/00
12/00
01/01
02/01
03/01
04/01
Rainfall (mm)
0
40
80
(d)
Potential pressure (cm-H2O)
-450
-300
-150
0
150
Tens @ 30 cm
Tens @ 110 cm
(c)
Potential pressure (cm-H2O)
-180
0
180
Tens @ 20 cm
Tens @ 100 cm
Phase 1
Phase 2
Phase 3
(b)
Stream discharge (m3/h)
100
50
0
675
140
127
280
438
389
(a)

 doi:10.2136/vzj2012.0054

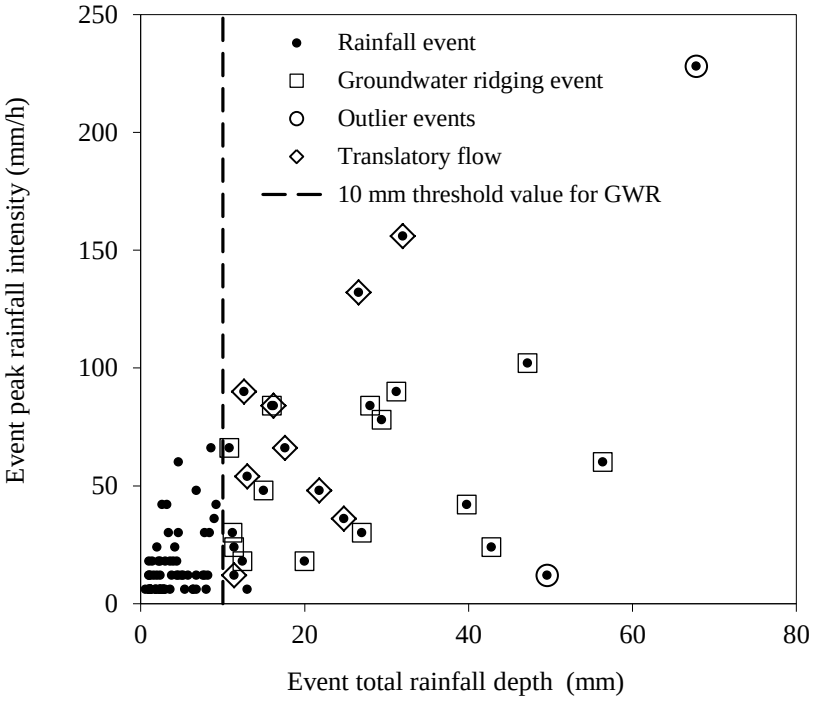

 doi:10.2136/vzj2012.0054

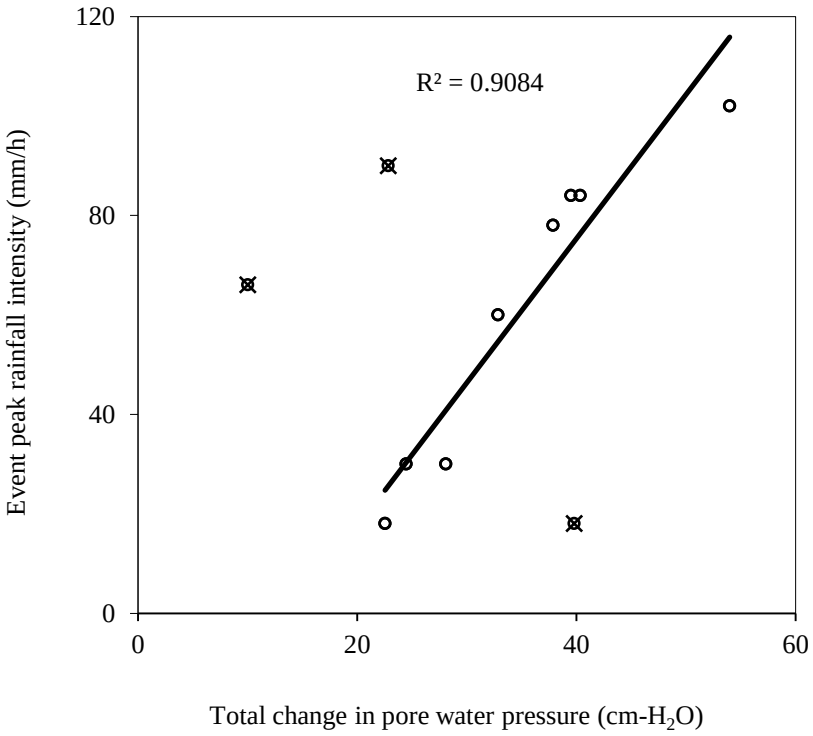

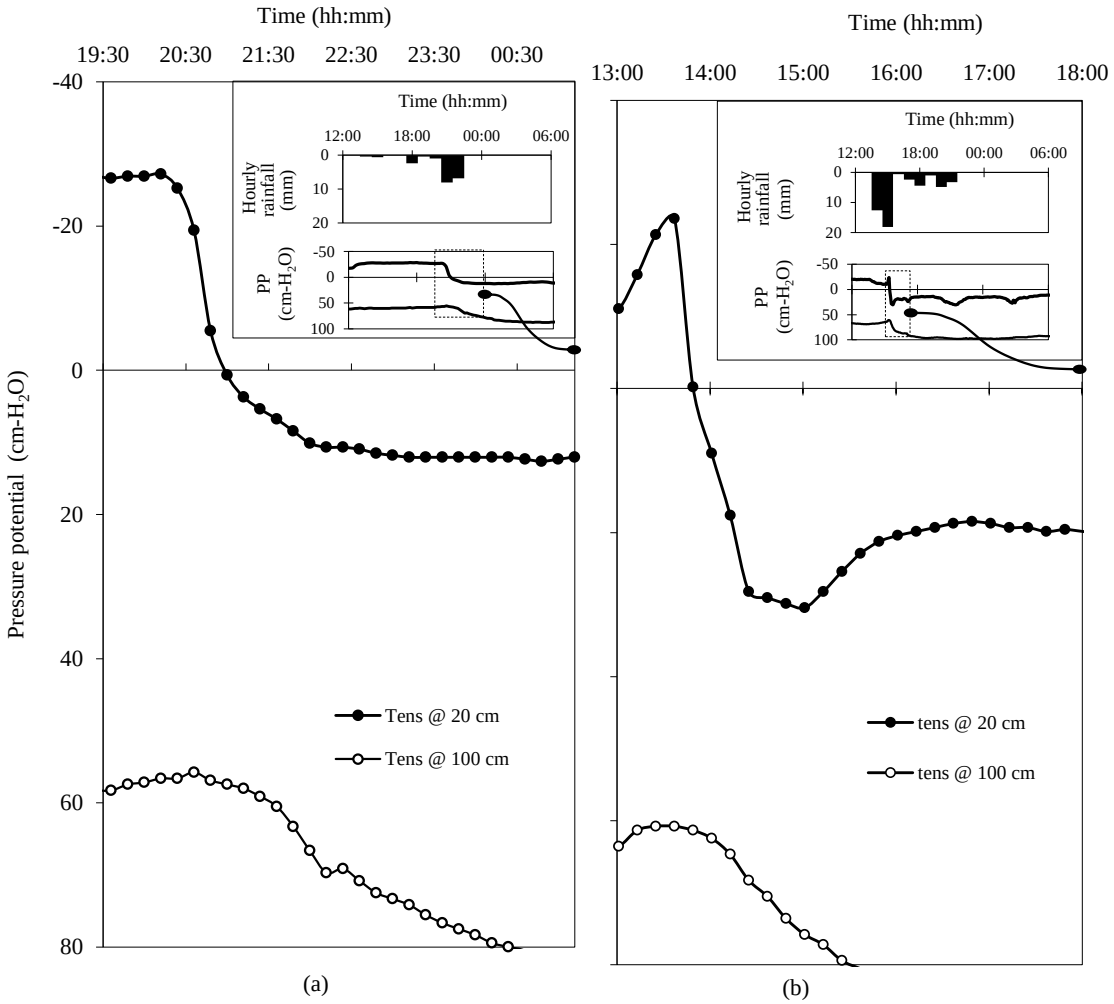
Time (hh:mm)
19:30
20:30
21:30
22:30
23:30
00:30
-40
-20
0
20
40
60
80
Pressure potential (cm-H2O)
Time (hh:mm)
12:00
18:00
00:00
06:00
Hourly rainfall (mm)
0
10
20
PP (cm-H2O)
-50
0
50
100
Tens @ 20 cm
Tens @ 100 cm
(a)
Time (hh:mm)
13:00
14:00
15:00
16:00
17:00
18:00
Time (hh:mm)
12:00
18:00
00:00
06:00
Hourly rainfall (mm)
0
10
20
PP (cm-H2O)
-50
0
50
100
tens @ 20 cm
tens @ 100 cm
(b)

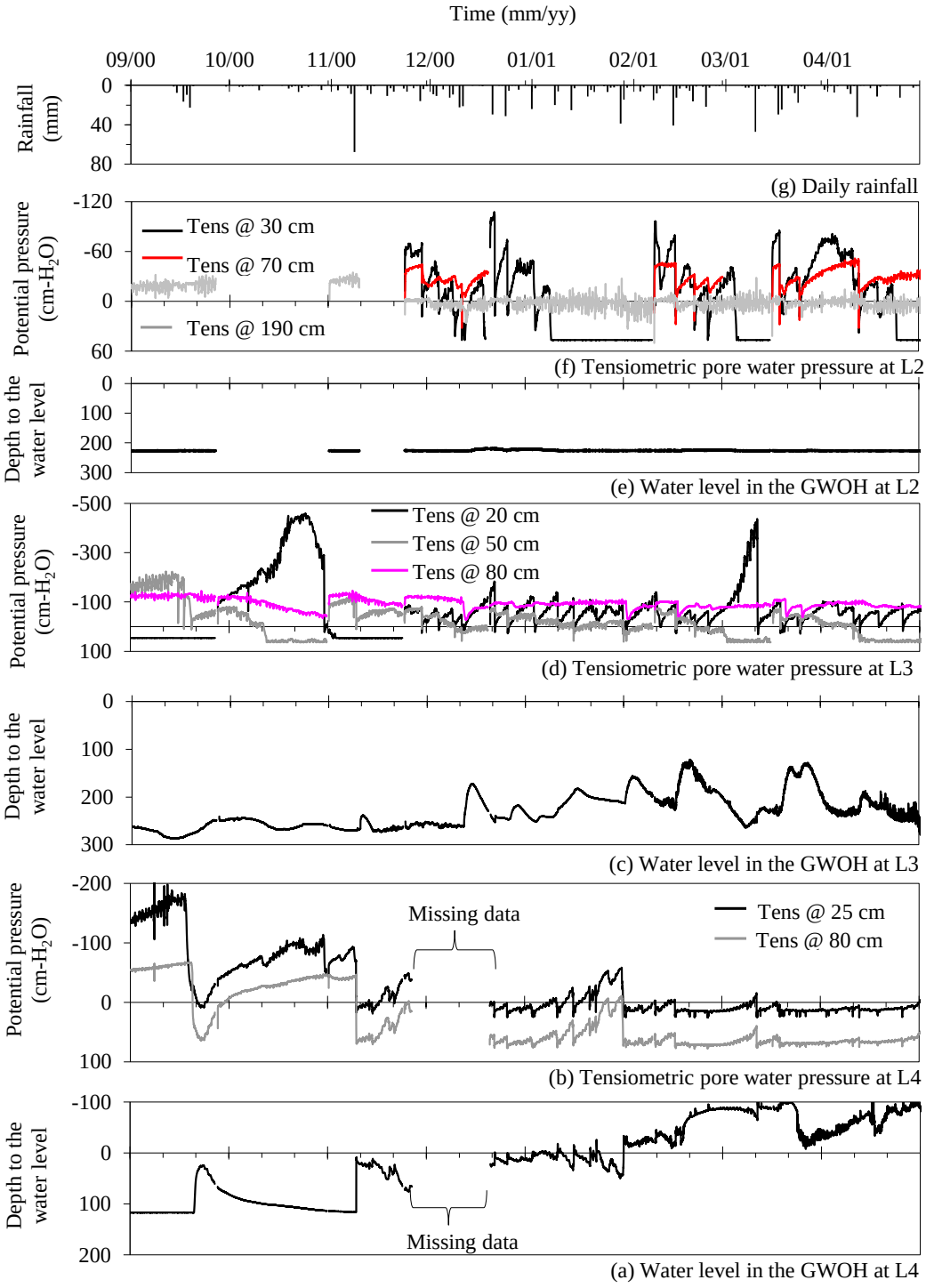
Time (mm/yy)
09/00
10/00
11/00
12/00
01/01
02/01
03/01
04/01
Rainfall (mm)
0
40
80
(g) Daily rainfall
Potential pressure (cm-H2O)
-120
-60
0
60
Tens @ 30 cm
Tens @ 70 cm
Tens @ 190 cm
(f) Tensiometric pore water pressure at L2
Depth to the water level
0
100
200
300
(e) Water level in the GWOH at L2
Potential pressure (cm-H2O)
-500
-300
-100
100
Tens @ 20 cm
Tens @ 50 cm
Tens @ 80 cm
(d) Tensiometric pore water pressure at L3
Depth to the water level
0
100
200
300
(c) Water level in the GWOH at L3
Potential pressure (cm-H2O)
-200
-100
0
100
Missing data
Tens @ 25 cm
Tens @ 80 cm
(b) Tensiometric pore water pressure at L4
Depth to the water level
-100
0
100
200
Missing data
(a) Water level in the GWOH at L4

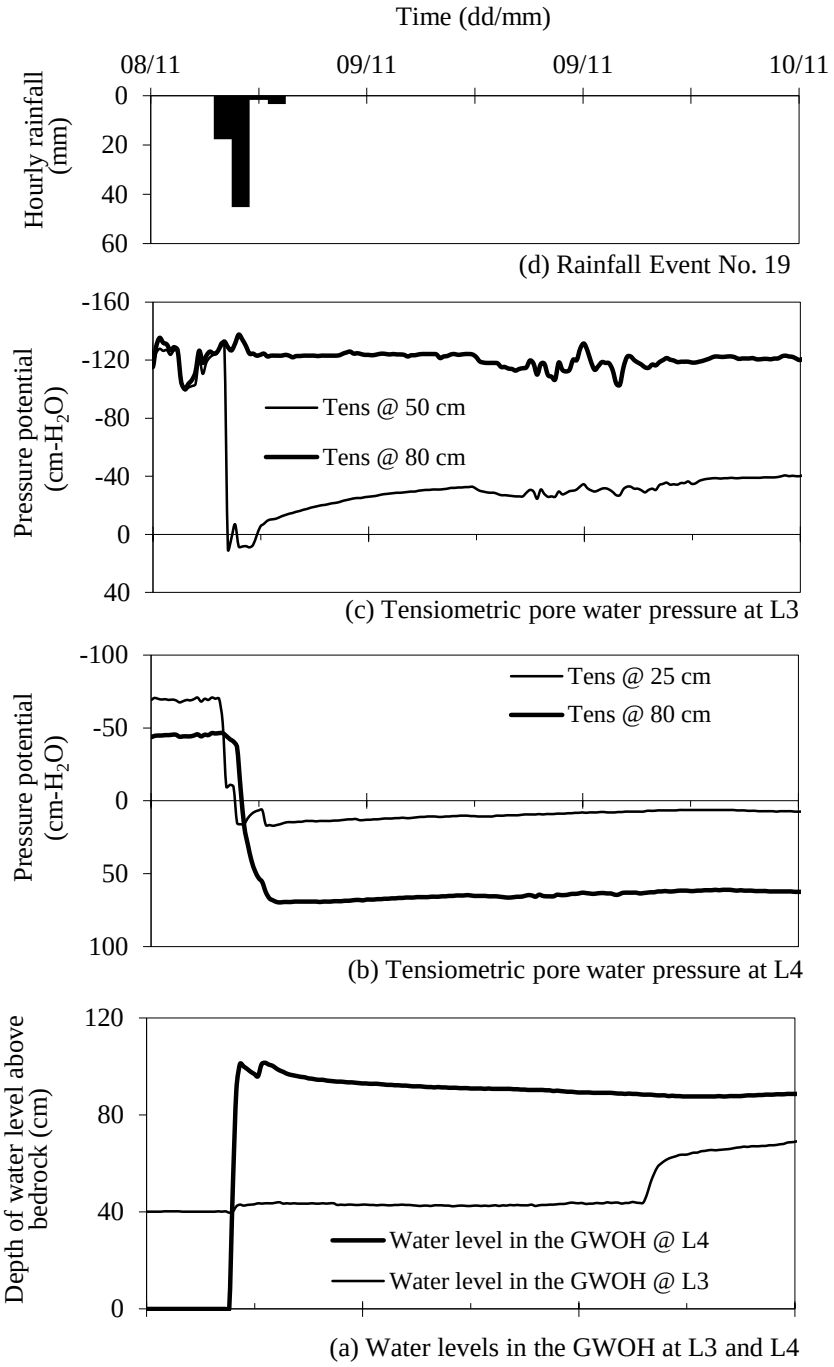

(d) Rainfall Event No. 19

(c) Tensiometric pore water pressure at L3

(b) Tensiometric pore water pressure at L4

(a) Water levels in the GWOH at L3 and L4

 doi:10.2136/vzj2012.0054

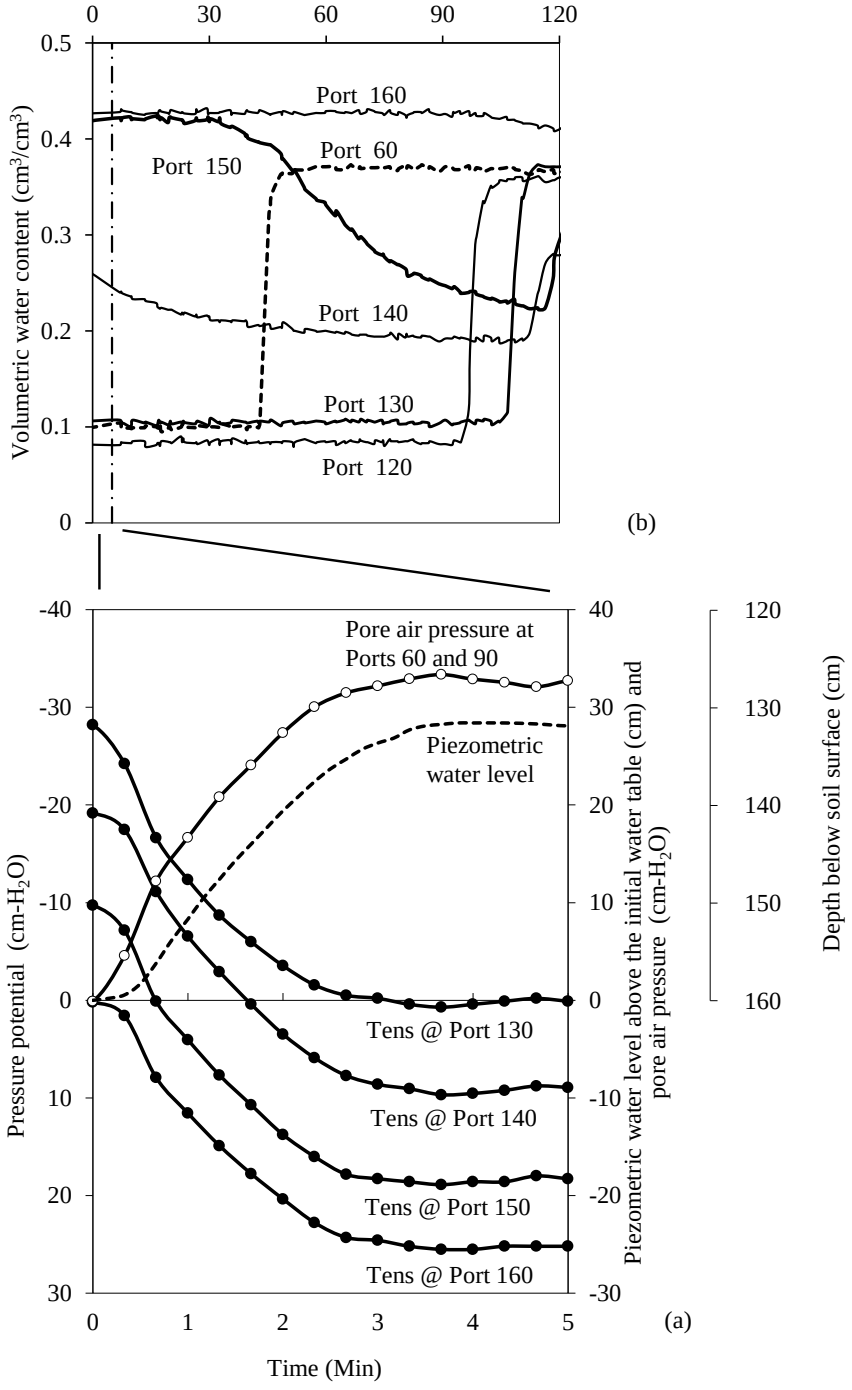

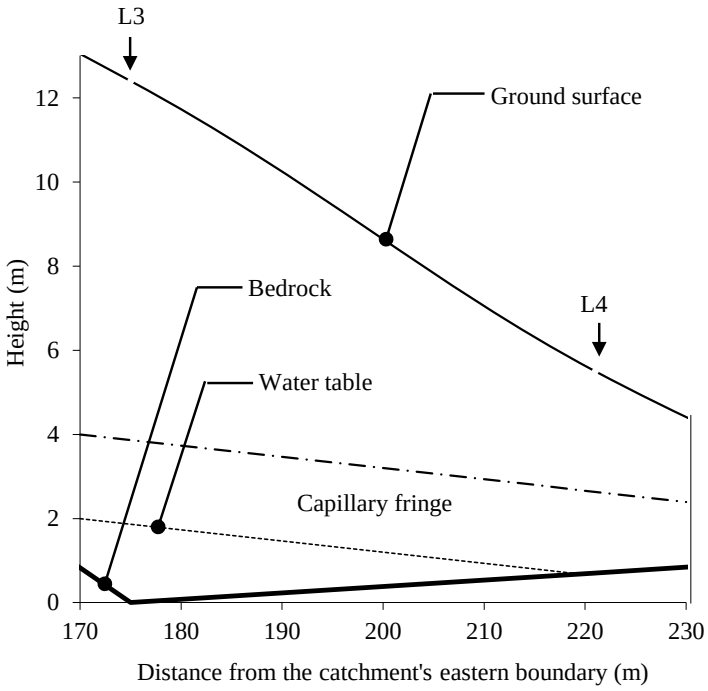
L3
Ground surface
L4
Bedrock
Water table
Capillary fringe
Height (m)
0
2
4
6
8
10
12
170
180
190
200
210
220
230
Distance from the catchment's eastern boundary (m)

 doi:10.2136/vzj2012.0054

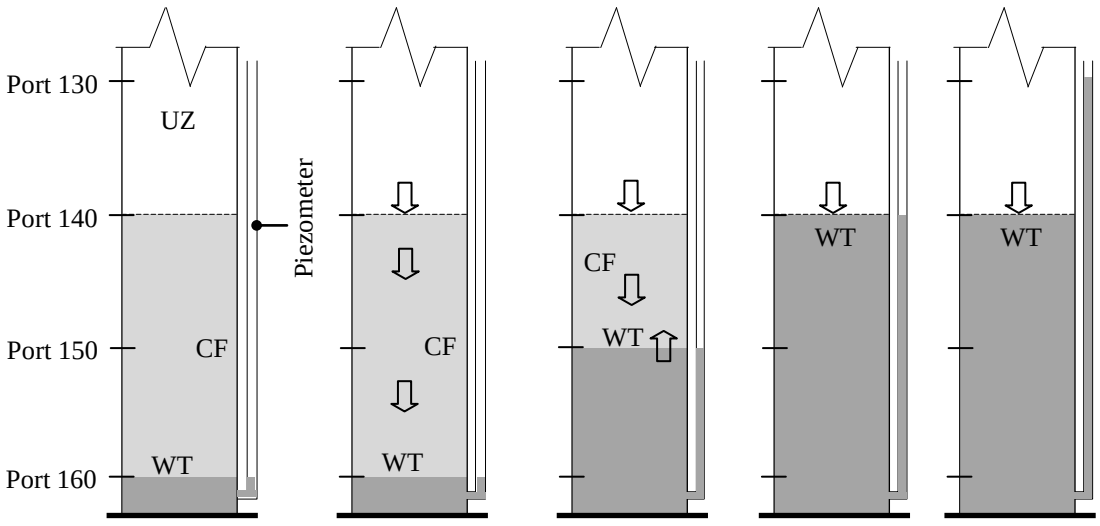

(a) $t = 0$ (b) $0 < t < 0.33$ (c) $t = 0.67$ (d) $t = 1.67$ (e) $t = 3.00$

 doi:10.2136/vzj2012.0054

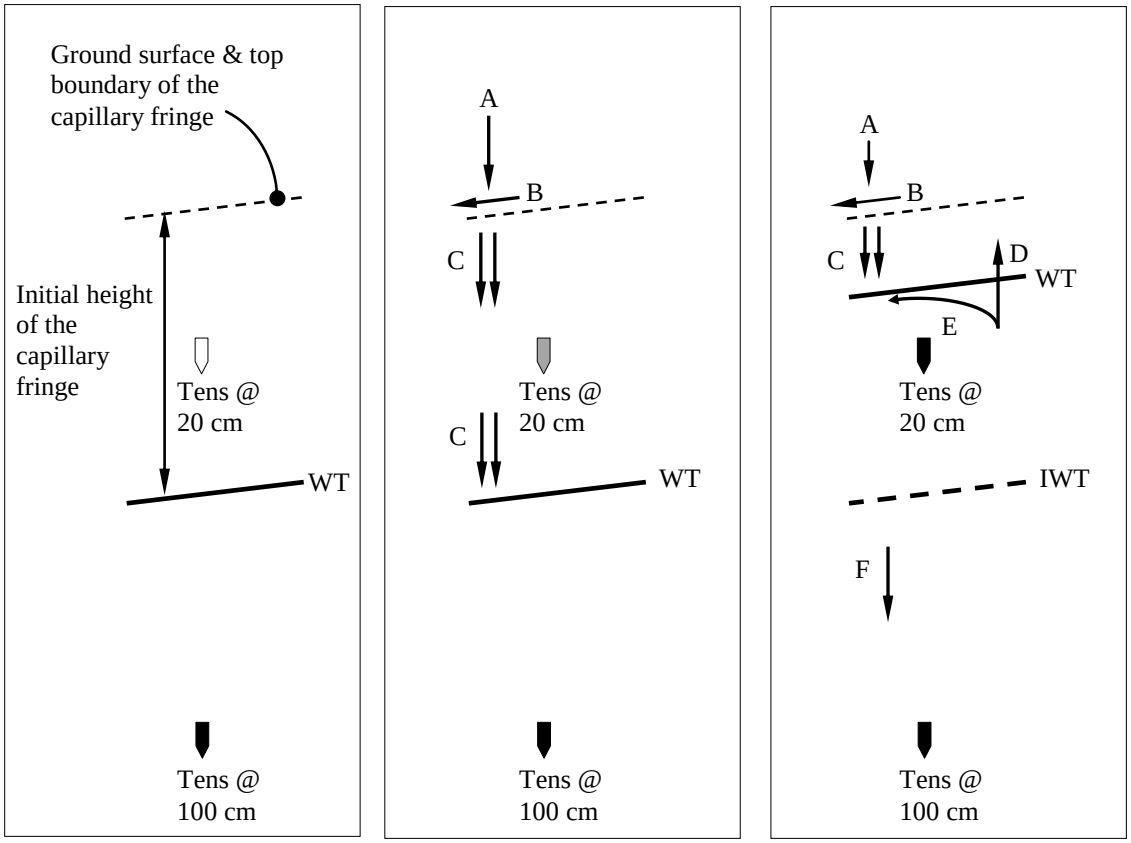

(a) 19:30 (b) 20:30 (c) 21:30

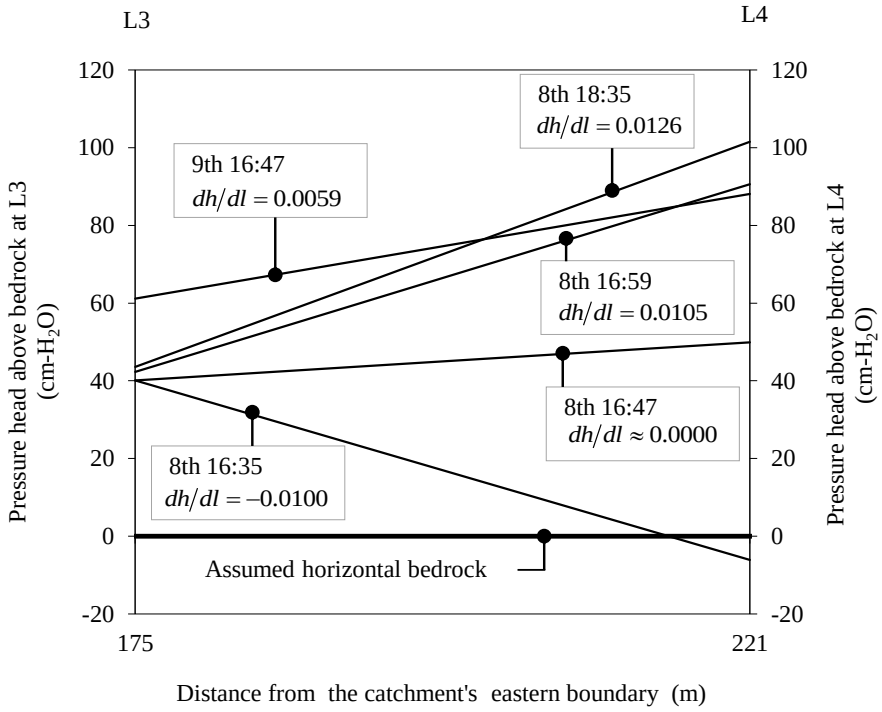
L3
L4
120
100
80
60
40
20
0
-20
8th 18:35
dh/dl = 0.0126
9th 16:47
dh/dl = 0.0059
8th 16:59
dh/dl = 0.0105
8th 16:47
dh/dl ≈ 0.0000
8th 16:35
dh/dl = −0.0100
Assumed horizontal bedrock
Pressure head above bedrock at L3 (cm-H2O)
Pressure head above bedrock at L4 (cm-H2O)
175
221
Distance from the catchment's eastern boundary (m)